

# Relict soil evidence for post-Miocene aridification in the Atacama Desert of South America

Ronald Amundson<sup>1,†</sup>, Arjun Heimsath<sup>2</sup>, Matt Jungers<sup>2,3</sup>, Simona Balan<sup>1,4</sup>, Angela Ebeling<sup>1,5</sup>, Kunihiko Nishiizumi<sup>6</sup>, Stephanie Ewing<sup>7</sup>, David Shuster<sup>8,9</sup>, Marc W. Caffee<sup>10</sup>, Marco Pfeiffer<sup>11</sup>, and William E. Dietrich<sup>8</sup>

<sup>1</sup>Department of Environmental Science, Policy, and Management, University of California, Berkeley, 120 Mulford Hall, Berkeley, California 94720, USA

#### **ABSTRACT**

Deep exposures of soil profiles on Miocene or Mio-Pliocene alluvial deposits were studied along a 500 km N-S transect in the Atacama Desert. These ancient deposits, with excellent surface preservation, now stand many meters above a broad incised Plio-Pleistocene alluvial terrain. Total geochemical analyses and mass balance calculations allowed the establishment of elemental gains, losses, and redistribution in the soils. From north to south (presently hyperarid to arid), the ancient soils reveal an increase in losses of rock-forming elements (Si, Al, Fe, K, Mg). Additionally, rare earth elements (REE) show losses with increasing southerly latitude and systematic patterns with soil depth. Some REEs appear to be unique chemical tracers of exogenous dust and aerosol additions to the soils. The removal of major elements and REEs is impossible in the present climate (one of salt and dust accumulation), revealing that for a significant period following the deposition of the alluvium, soils were exposed to rainfall, chemical weathering, and mass loss—with a geographical pattern that mirrors the present rainfall gradient in

Ronald Amundson https://orcid.org/0000-0003 -1510-7313 †earthy@berkeley.edu the region. Following the cessation of weathering, the pre-weathered soils have undergone enormous dust and salt accumulations, with the rates and types of salt accumulation consistent with latitude: (1) carbonate in the south and (2) sulfate, chlorides, and nitrates to the north. The quantity, and apparent rates, of salt accumulation have a strong latitudinal trend. Isotopes of sulfate have predictable depth patterns based on isotope fractionation via vertical reaction and transport. The relict hyperarid soils are geochemically similar to buried Miocene soils (ca. 10-9 Ma) in the region, but they differ from older Miocene soils, which formed in more humid conditions. The overall soil record for the Atacama Desert appears to be the product of changes in Pacific Ocean sea surface temperatures over time, and resulting changes in rainfall. The mid-Miocene was relatively humid based on buried soil chemistry and evidence of fluvial activity. The mid to late Miocene cooling (ca. 10-5.5 Ma) appears to have aridified the region based on paleosol soil chemistry. Pliocene to earliest Pleistocene conditions caused weathering of the relict soils examined here, and regional fluvial activity. Since the earliest Pleistocene, the region has largely experienced the accumulation of salts and, except for smaller scale oscillations (glacial-interglacial), has experienced protracted hyperaridity.

#### INTRODUCTION

Chile is well known as a natural laboratory for studying the effect of rainfall on terrestrial surface processes (e.g., Bernhard et al., 2018; Ewing et al., 2006, 2007, 2008a, 2008b; Owen et al., 2011; Navarro-González et al., 2003; Oeser and von Blanckenburg, 2020; Quade et al., 2007; Rech et al., 2003). From south to north, rainfall steadily declines, reaching near zero values in the far north, near the border with Peru. In terms of the rainfall impact on soils, Ewing et al. (2006) examined the chemistry of Plio-Pleistocene soils from the southern periphery of the present Atacama Desert near Copiapo, which is presently at the hyperarid/arid climate boundary, northward to near Antofagasta, which is well within a hyperarid climate setting. The contents of salts, isotope chemistry of various compounds, and other soil features varies predictably and systematically with decreases in rainfall (Fig. 1). This work revealed previously unrecognized depth-dependent isotope fractionating processes that impact S, O, and Ca isotopes in sulfate (Ewing et al., 2008a), N and O isotopes in nitrate (Welsh et al., 2020), and Cl in halite (Amundson et al., 2012b). All these studies were done on soils formed in nominally late Pliocene-early Pleistocene alluvial deposits, a vast and regional expanse of sediments that appear to have occurred in concert with an erosional stripping of silicate soil mantled hillslopes, and the

*GSA Bulletin*; January/February 2025; v. 137; no. 1/2; p. 465–480; https://doi.org/10.1130/B37356.1. Published online 31 July 2024

<sup>&</sup>lt;sup>2</sup>School of Earth and Space Exploration, Arizona State University, Tempe, Arizona 85287, USA

<sup>&</sup>lt;sup>3</sup>Department of Geosciences, Denison University, Granville, Ohio 43023, USA

<sup>&</sup>lt;sup>4</sup>California Department of Toxic Substances Control, 700 Heinz Avenue, Berkeley, California 94710, USA

<sup>&</sup>lt;sup>5</sup>Wisconsin Lutheran College, Milwaukee, Wisconsin 53226, USA

<sup>&</sup>lt;sup>6</sup>Space Sciences Laboratory, University of California, Berkeley, 7 Gauss Way, Berkeley, California 94709, USA

<sup>&</sup>lt;sup>7</sup>Department of Land Resources and Environmental Sciences, Montana State University, Bozeman, Montana 59717, USA

<sup>&</sup>lt;sup>8</sup>Earth and Planetary Science, University of California, Berkeley, McCone Hall, Berkeley, California 94720, USA

<sup>&</sup>lt;sup>9</sup>Berkeley Geochronology Center, 2455 Ridge Road, Berkeley, California 94709, USA

<sup>&</sup>lt;sup>10</sup>Department of Physics and Astronomy and Department of Earth, Atmospheric, and Planetary Sciences, Purdue University, West Lafayette, Indiana 47907-2036, USA

<sup>&</sup>lt;sup>11</sup>Facultad de Ciencias Agronomicas, Universidad de Chile, Santiago, Chile

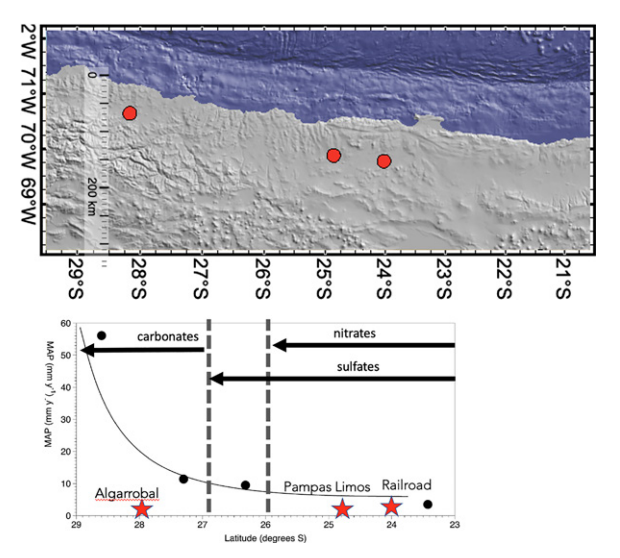


Figure 1. A very simple perspective of the climate and soil geochemistry changes with latitude in the study area. Four weather stations (black dots) provide mean annual precipitation (MAP) versus latitude: 1-Antofagasta,  $\sim$ 0 m above sea level (masl); 2—Chañaral,  $\sim$ 0 masl; 3—Copiapo, 383 masl; 4—Vallenar, 396 masl. Black arrows show general regions of salt accumulation in alluvial soils with latitude. The extent of major soil nitrate deposits is from Michalski et al. (2004). The three sites examined in this study are identified by red circles/stars.

onset of the (most recent?) period of protracted hyperaridity (Amundson et al., 2012a).

While the prominence of Plio-Pleistocene deposits is impressive, there remain large expanses of higher standing gravelly fluvial deposits, commonly called the "Atacama gravels," or what is also considered part of the "Atacama pediplain" (Muñoz-Farías et al., 2023). These fluvial fills required significant runoff to drive the deposition of these deposits, and later their subsequent incision (Mortimer, 1973; Muñoz-Farías et al., 2023). As Evenstar et al. (2017) noted for landforms to the north of our study area, these ancient gravelly surfaces are possibly time-transgressive, forming at differing times depending on local tectonics, climate, and hydrology. In a number of locations, these Miocene sedimentary deposits exhibit impressive degrees of preservation, with negligible erosion or surface alteration. Thus, an interesting question is whether the geochemistry of the soils weathered into these ancient geomorphic surfaces record soil formation in a continuous and broadly stable rainfall regime, or whether they contain geochemical evidence of variations in rainfall over millions of years.

As a starting hypothesis, we anticipated spatial rainfall variations due to present rainfall gradients.

We also anticipated rainfall variations over time, due to the global climatic processes that impact the region. In particular, post-Pliocene changes in Pacific circulation are proposed to have shifted regional climate from a permanent El Niño-like condition to the present El Niño-Southern Oscillation (ENSO) cycling (Ford et al., 2015; Wara et al., 2005). Additionally, Pleistocene glacial-interglacial transitions certainly impacted rainfall in the high-elevation Andean plateau (de Porras et al., 2017), and may have also impacted rainfall in the lower elevation desert regions to the west, the area examined here.

Over a number of years of work, we have been able to discover and sample deep, well-exposed soil exposures in prominent Miocene landforms along a 450 km N to S transect. The southernmost of these was discussed in a recent paper (Ebeling et al., 2016). Here, we add soils to the north to assemble a Miocene latitude gradient (climate gradient) of relict soils in northern Chile. The term "relict" indicates that the soil has persisted through multiple environmental oscillations. We use a combination of geochemical and field observations to examine rates of landscape alteration and investigate information embedded in the soils about climatic history. These soils, due to our ability to examine

deep and complete profiles, greatly enhance our understanding of pedological patterns and climate history in this unique region on Earth and provide methods to extract climate information from other arid regions on Earth.

#### **METHODS**

#### **Site Description**

To begin, a general overview of modern soilforming patterns in northern Chile is presented (Fig. 1). From south to north, rainfall declines from  $\sim$ 32 mm y<sup>-1</sup> at Vallenar, to 3.5 mm y<sup>-1</sup> in Antofagasta. Habitations with weather stations are along river channels and/or on the coast. It is possible that rainfall may be lower in the interior, where some of our sites are located (red stars in Fig. 1). From  $\sim 26.1^{\circ}$ S to the north, soils contain significant nitrate accumulations. Nitrates may extend farther south, but the concentrations decline considerably with southerly latitude. Sulfates are prominent accumulations to 27°S, and begin to decline in importance (but are still found) to the south. From ~27°S to 29°S (and beyond), carbonates are prominent pedogenic accumulations. This general pattern represents zones where these salts are major accumulations, and smaller quantities can accumulate outside of these broad limits.

On hillslopes, there are three broad zones of hillslope soil processes and conditions. From  $\sim 26^{\circ}$ S northward, hillslopes are mantled with soils derived from significant amounts of dust and atmospheric salts. These tend to overlie fresh bedrock, suggesting that the previous soil mantle was stripped by erosion prior to the emplacement of the salts and dust (Owen et al., 2011). There is a narrow and discontinuous latitudinal band of hillslopes where only a very thin (mm to cm) soil cover overlies bedrock, due to present erosion rates that tend to match or exceed soil production rates (Owen et al., 2011). Finally, south of this narrow zone, soils derived from the disintegration of the underlying rock reappears on hillslopes, mixed with salts, especially carbonate. Very roughly, 26°S is the biotic (presence of plants to the south) versus abiotic (absence of plants to the north) boundary in the region. Irregularities occur due to elevation and other geographical factors that influence both salt deposition and plants.

The southernmost site examined here (Algarrobal; Table 1; Figs. 2A and 2B) is an alluvial fan mapped as "Tertiary gravas de Atacama" in Moscoso et al. (1982). It is located on a highway exposure along the Pan American Highway at 480 m above sea level (masl). The original exposure (observed in 2006) has been destroyed by subsequent highway expansion. The ancient

TABLE 1. STUDY SITE INFORMATION

Site	Latitude (°S)	Longitude (°W)	MAP* (mm)	MAT* (°C)	Elevation (masl)	Approximate age <sup>†</sup>
Algarrobal	28.158953	70.641705	~21	$\sim$ 15	480	0.7-1.4 Ma (10Be/26AI)
Pampas Limos	24.852457	69.876041	$\sim$ 5	$\sim$ 11	2100	4.9+ Ma (10Be/26AI)
Railroad	24.019598	69.772199	$\sim$ 4	$\sim$ 14	1012	5.4-7 Ma ( <sup>21</sup> Ne), 4-5.3 Ma ( <sup>10</sup> Be/ <sup>26</sup> Al)

Note: MAP—mean annual precipitation; MAT—mean annual temperature; masl—m above sea level. \*Based on linear extrapolation, by latitude, between climate stations illustrated in Figure 1. These extrapolations do not account for the unknown effect of elevation on rainfall. A local lapse rate of 2 °C/1000 m (based on Antofagasta = 0 masl; Escondido = 3100 masl) was used for the elevation corrections to MAT. The elevation of Algarrobal is similar to the nearby station at Vallenar.

†See text for more information

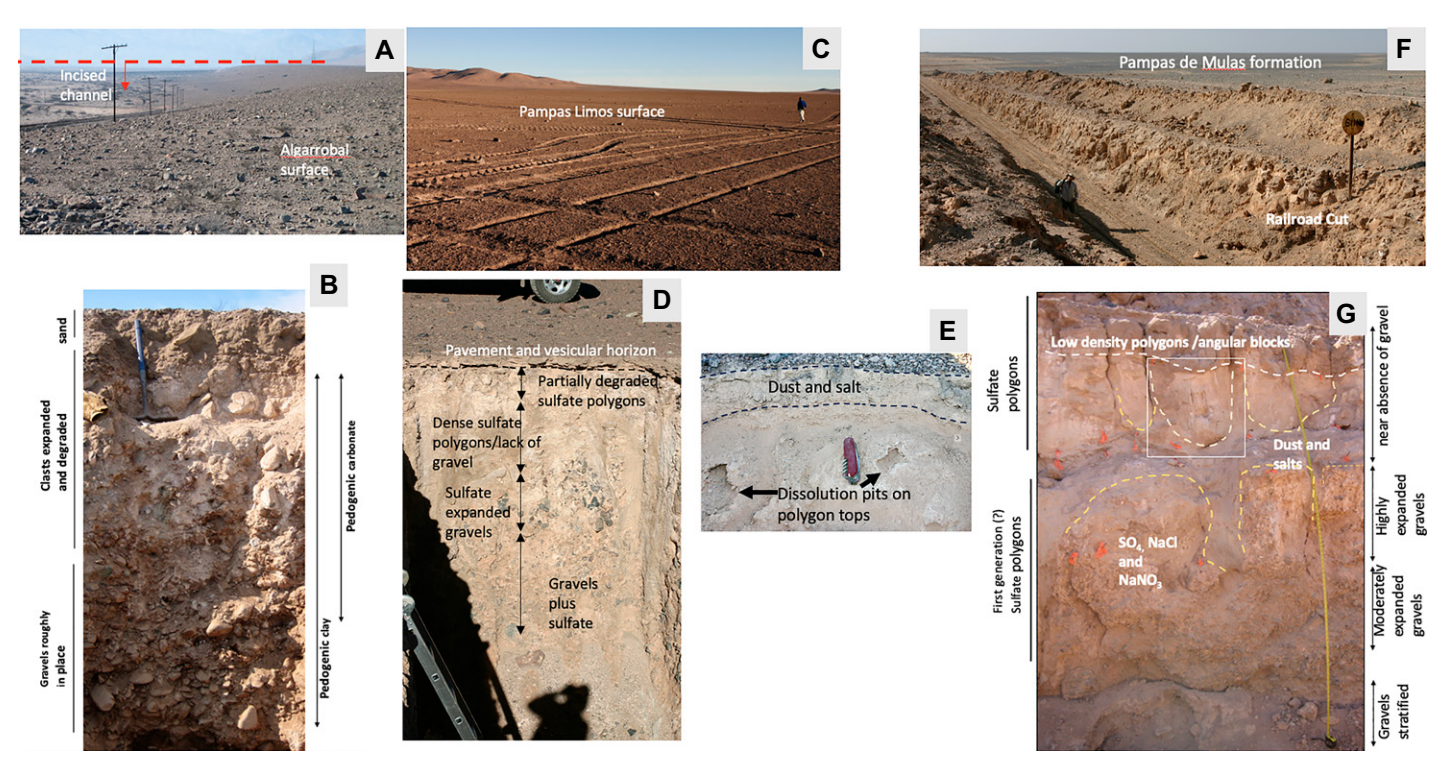


Figure 2. Photographs of landforms and soils examined in study. (A) The Tertiary gravas de Atacama surface and the incision into the adjacent and younger landforms. (B) Soil formed into the surface in part A. (C) The Pampas Limos surface (note wheel tracks imbedded into soft surficial dust-rich vesicular layer). (D) Soil formed into surface in part C. (E) A close-up of the contact between the pavement/vesicular surface layer and underlying sulfate polygons, illustrating dissolution pits etched into polygon tops, and now apparently being overlain by dust and salts. (F) The Pampas de Mulas formation and the railroad excavation through it. (G) A cleaned and logged profile of soil formed into the landform in part F.

geomorphic surface stands >20 m above a wide channel that is incised into the landscape. The second site (Pampas Limos) is located at 2100 m on a Miocene fan, with the map unit *Tac* ("Ancient/Tertiary alluvial and colluvial deposits"; Marinovic et al., 1992) exposed by numerous 3 m+ deep trenches created during Chilean highway construction (Figs. 2C-2E). This soil was sampled in 2006. The third site (Railroad) is a deep cross-sectional exposure of a Miocene alluvial deposit ("Tertiary Pampa de Mulas Formation"; Marinovic et al., 1992) made by an early(?) twentieth century railroad construction (Figs. 2F and 2G). As the name of the formation (Mule Plain) suggests, the land surface is traced by remarkably visible tracks made by nineteenth century mule-pulled nitrate carts, attesting to the extreme aridity and slowness of surficial alteration processes. This site, at 1012 masl, was sampled in 2008. The significant differences in elevation between the sites certainly impacts temperatures and fog frequency. The 1000 m elevation is commonly cited as an approximate upper boundary for the near daily coastal fog incursions into the desert (Cereceda et al., 2008). We have observed fog at the two endmembers of the transect, which lie just above or below 1000 m.

## Field and Laboratory Methods

Soil profiles samples were collected from preexisting excavations. Surfaces were cleaned with a rock hammer or pick, and pedogenic horizons were identified and marked in the field. Samples (integrating over the entire horizon) were placed in sealable plastic bags. In the field, gravels were coarsely separated and weighed relative to the "non-gravel" material. In the laboratory, samples were sieved and additional >2 mm material was added to field-based coarse fragment measurements.

For <sup>10</sup>Be and <sup>21</sup>Ne depth profiles at the Railroad location, soil was collected separately at regular intervals from the land surface to depths of 75–200 cm. Samples were first sieved to extract the 250–1000 μm fraction, and grain sizes larger than 1000 μm were then crushed and sieved to augment the total sample in the 250–1000 μm range. This procedure was needed since they were not quartz-rich. Quartz was isolated via cleaning in aqua regia and subsequent etching in HF and HNO<sub>3</sub> (Kohl and Nishiizumi, 1992). Beryllium was extracted and purified using anion and cation exchange columns and acetylacetone solvent extraction. The <sup>10</sup>Be/<sup>9</sup>Be

was measured at the PRIME Lab, Purdue University (Sharma et al., 2000). The measurements were normalized to Be and Al accelerator mass spectrometry standards (Nishiizumi, 2004; Nishiizumi et al., 2007). Cosmogenic <sup>21</sup>Ne was measured at the Berkeley Geochronology Center by encapsulating 150 mg aliquots (of the same purified quartz analyzed for 10Be) in a Ta packet, heating them under vacuum using a 150W diode laser, purifying the released gas by reaction with hot and/or cold getters and cryogenic separation of Ne from other noble gases, and analyzing the resulting Ne in a MAP-215-50 mass spectrometer. Balco and Shuster (2009) describe analytical details. Analyses of the CRONUS-A quartz standard (320  $\pm$  11  $\times$  10<sup>6</sup> atoms g<sup>-1</sup>; Vermeesch et al., 2015) during the period of these measurements yielded a cosmogenic 21Ne concentration of 338.9  $\pm$  3.8  $\times$  10<sup>6</sup> atoms g<sup>-1</sup>.

For surface exposure dating, silicate rock or quartz samples were crushed, milled, and sieved before quartz purification by HF and  $\rm HNO_3$  leaching, yielding  $\sim 20-300~\rm g$  of clean quartz (Kohl and Nishiizumi, 1992). The chemical and measurement procedures were the same as those employed for the depth profile samples. The results were converted to minimum expo-

TABLE 2. COSMOGENIC NUCLIDE DEPTH PROFILE DATA FOR MODERN CHANNEL AND YUNGAY\* AND FOR THE RAILROAD SOIL CONSIDERED HERE

Latitude (°S)	Longitude (°W)	Altitude (masl)	Depth (cm)	<sup>10</sup> Be (10 <sup>6</sup> atoms/g)	<sup>21</sup> Ne (10 <sup>7</sup> atoms/g)	<sup>21</sup> Ne "age"— surface exposure (10 <sup>6</sup> yr)	<sup>21</sup> Ne "age"— constant depth (10 <sup>6</sup> yr)	
Modern channel (Jungers et al., 2013)								
23.77	70.25	614	Ó	$\textbf{3.73} \pm \textbf{0.08}$	$\textbf{5.72} \pm \textbf{0.38}$	_	_	
			25	$\textbf{3.96} \pm \textbf{0.12}$	$\textbf{6.24} \pm \textbf{0.31}$	_	_	
			50	$4.27 \pm 0.13$	$6.41 \pm 0.32$	_	_	
			75	$4.66 \pm 0.20$	$5.30 \pm 0.23$	_	_	
Railroad	(this study)							
24.02	69.77	1012	0	$\textbf{8.16} \pm \textbf{0.21}$	$19.53 \pm 0.77$	4.74	4.74	
			75	$7.81\pm0.28$	$\textbf{23.59} \pm \textbf{0.93}$	5.75	12.8	
			100	$7.69 \pm 0.20$	$\textbf{22.26} \pm \textbf{0.88}$	5.42	15.7	
			150	$5.91 \pm 0.18$	$\textbf{19.84} \pm \textbf{0.79}$	4.82	23.7	

Note: masl—m above sea level. \*Jungers et al. (2013).

sure ages and maximum erosion rates using the production rate scaling factors of Lal (1991) and default values for all parameters (Vermeesch, 2007) from site-specific location data. The results for samples collected in 2004 and 2005 are shown in Table 2.

The numerical framework to interpret exposure time of analyzed samples is as follows. Surface exposure age of clasts:

$$N_{t} = N_{o}e^{-\lambda t} + \frac{P_{o}}{\lambda + \mu \epsilon} \left( 1 - e^{-(\lambda + \mu \epsilon)t} \right); \qquad (1)$$

and depth profiles assuming constant soil thickness (Jungers et al., 2013):

$$N_{z,t} = N_o e^{-\lambda t} + \frac{P_o e^{-\rho z/\Lambda}}{\lambda + \left(\frac{\rho \varepsilon}{\Lambda}\right)} \left[1 - e^{-\left(\lambda + \left(\frac{\rho \varepsilon}{\Lambda}\right)\right)t}\right], \quad (2)$$

where N is the cosmogenic nuclide concentration (atoms  $g^{-1}$ ), t is time (y),  $N_o$  is the inherited concentration of cosmogenic radio-nuclides (CRNs),  $N_i$  is the radionuclide concentration of sediment deposited at the surface,  $\varepsilon$  is the erosion rate (cm  $y^{-1}$ ), z is depth below the surface (cm),  $P_o$  is the CRN production at the surface (atoms  $g^{-1}$   $y^{-1}$ ),  $\Lambda$  is the attenuation length for CRN production (g cm<sup>-2</sup>),  $\rho$  is sediment density (g cm<sup>-3</sup>), and  $\mu = \rho/\Lambda$ . Nuclide production rates ( $P_o$ ) vary with latitude and elevation; we used Lal's (1991) method to determine production rates at a latitude of 20°S, and the measured elevations, assuming a 2.50% muon contribution.

Ratios (R) of pairs of CRNs, such as <sup>26</sup>Al and <sup>10</sup>Be (used here in surface exposure dating) are useful means of identifying perturbations to assumed conditions of simple exposure histories. The calculated ratios of a given CRN pair are computed over a given time span using Cosmo-Calc 3.1 using the scaling factors of Lal (1991) and default values for all parameters (Vermeesch, 2007). If the measured R of a sample lies on the

projected trajectory, it suggests a simple exposure history. However, samples that lie below a projected pattern for R over time (including possible steady-state erosion) are indicative of a complex history, one involving possible erosion and/or burial and re-exposure (e.g., Lal, 1991).

Major elemental abundance was determined by ALS Global (Reno, Nevada, USA) using inductively coupled plasma—mass spectrometry (ICP-MS) and ICP-AES (atomic emission spectrometry) on a lithium-borate fusion of each soil sample. Total S was obtained using a Leco furnace and infrared spectroscopy. Inorganic C (carbonate) was determined by HCl leach and Leco-gasometric finish. Rare earth elements were determined in 2006 from a lithium metaborate fusion using ICP-MS (ALS, https://www.alsglobal.com/en/).

Sulfate was extracted based on methods published by Michalski et al. (2004) and Ewing et al. (2008a), with some modifications. Thirty-five grams of double distilled water was added to 50 ml centrifuge tubes (soil:water = 1:7). Tubes were shaken horizontally for four hours (low speed) and centrifuged at 3000 rpm for 30 min. A vacuum filter was used to separate soil from supernatant (into clean 50 ml centrifuge tube). The filters were rinsed with extractant solution (KH<sub>2</sub>PO<sub>4</sub>, pH 7). The tubes were put on a rack in a warm water bath, and 5 ml 1 M BaCl<sub>2</sub> was slowly added to solution to precipitate BaSO<sub>4</sub>. Six drops of 6N HCl were added to dissolve BaCO<sub>3</sub>. The tubes were centrifuged at 3000 rpm for 30 min, decanted, and dried. Splits of these were submitted for stable isotope analyses (next section). However, due to possible precipitation of nitrate, 0.05 M DTPA (diethylenetriamine pentaacetate) solution in a 1 M NaOH solution was mixed with barite crystals in a 1:500 weight ratio (e.g., ~30 mg in 15 ml DTPA solution). The solution was shaken vigorously until all the barite dissolved. Then, 10 drops of 10 M HCl was added to lower the pH to 3-4 and to reprecipitate barite (which takes up to 1 h). The suspension was centrifuged, decanted, and oven dried.

The changes (gains/losses) in soil (<2 mm fraction) geochemistry were determined using the mass balance method presented by Nesbitt (1979) and Brimhall and Dietrich (1987):

$$tau(\tau) = \left[ (C_{m,s}/C_{i,s})/(C_{m,p}/C_{i,p}) \right] - 1, \quad (3)$$

where C = elemental concentrations and the subscript m = mobile element, i = immobile element, s = soil, and p = parent material. The choice of an immobile element in fluvial deposits can be challenging. In the main body of the text, the choice of reference elements is discussed in detail.

The total S concentration and  $\delta^{34}$ S values of soils and the  $\delta^{34}$ S value of sulfate in water samples were determined using the SO<sub>2</sub> EA-combustion-IRMS method on a GV Isoprime isotope ratio mass spectrometer coupled with an Eurovector Elemental Analyzer (model EuroEA3028-HT) at the Laboratory for Environmental and Sedimentary Isotope Geochemistry (LESIG), University of California at Berkeley. Briefly, a small amount of powdered sample containing a minimum of 2 μg S mixed with V<sub>2</sub>O<sub>5</sub> catalyst was thermochemically decomposed with copper wires at 1020 °C, and the isotopic composition of the resulting SO<sub>2</sub> gas was measured. Water vapor was removed with a Mg(ClO<sub>4</sub>)<sub>2</sub> trap and CO<sub>2</sub> was eluted out using a dilutor. Several replicates of the international standard NBS127 and two lab standards (both pure BaSO<sub>4</sub>) were run with each batch of samples. The long-term analytical precision of this method is better than 0.2%. Sulfate for O isotopes was weighed into silver capsules and combusted in continuous flow using an Elementar PYRO Cube interfaced with a Thermo Delta V mass spectrometer. Long-term precision for IAEA-V-9 cellulose is  $\pm 0.20\%$ .

#### RESULTS AND DISCUSSION

# **Landform Ages**

## Landform Ages: Results

Cosmogenic radio-nuclide measurements of surface samples of quartz clasts and quartz from silicate gravels were made at (or on the same mapped landform) at all three locations (Table 3). Figure 3 illustrates the data on a plot of <sup>26</sup>Al/<sup>10</sup>Be versus <sup>10</sup>Be, an evolution diagram in which the abscissa is a proxy for exposure age. The samples from the two driest locales (Railroad and Pampas Limos) are near CRN saturation (Table 3); i.e., production and decay are in equilibrium. These data points are close to projected CRN evolution curves indicating little or no erosion (Fig. 3). The exposure ages of surface

TABLE 3. COSMOGENIC RADIONUCLIDE DATA FOR SURFACE SAMPLES ANALYZED FOR E	EXPOSURE DATING

Sample	Latitude (°S)	Longitude (°W)	Altitude (m)	Scaling factor	<sup>10</sup> Be (10 <sup>6</sup> atom/g)	<sup>26</sup> AI (10 <sup>6</sup> atom/g)	Minimum <sup>10</sup> Be age (Ma)	Maximum erosion rate (m/m.y.)	Reference
Algarrobal CB 04-6 CB 04-7 CB 04-8	28.16 28.16 28.16	71.05 71.05 71.05	171 171 171	0.919 0.909 0.919	$\begin{array}{c} 2.84 \pm 0.04 \\ 2.53 \pm 0.05 \\ 4.77 \pm 0.09 \end{array}$	$14.18 \pm 0.75 \\ 10.87 \pm 0.83 \\ 13.21 \pm 0.93$	$0.7 \pm 0.1 \\ 0.6 \pm 0.2 \\ 1.4 \pm 0.4$	0.7 0.9 0.3	This work This work This work
Pampas Limos CG 04-1 CG 05-1	24.68 24.85	69.88 69.89	2133 2139	3.487 3.512	$\begin{array}{c} 32.0 \pm 1.0 \\ 35.8 \pm 1.4 \end{array}$	$\begin{array}{c} \textbf{116.4} \pm \textbf{2.9} \\ \textbf{119.8} \pm \textbf{3.9} \end{array}$	$\begin{array}{c} 4.9 \pm 0.7 \\ \text{Saturated} \end{array}$	0.03 0.01	Amundson et al. (2012a) Amundson et al. (2012a)
Railroad CHM 05-1 CHM 05-2	24.04 24.05	69.78 69.81	1010 960	1.574 1.518	$14.7 \pm 0.3 \\ 13.2 \pm 0.3$	$43.5 \pm 2.1 \\ 48.4 \pm 2.0$	$5.3\pm0.6\\4.0\pm0.2$	0.02 0.05	Amundson et al. (2012a) Amundson et al. (2012a)

clasts indicate minimum exposure ages of Pampas Limos and Railroad of 4.9 Ma and 5.3 Ma, respectively. The Algarrobal samples were collected on the same mapped geologic unit that the soil formed in, but at a location 40 km to the west. In contrast to the samples from Railroad and Pampas Limos, the Algarrobal samples are well below the evolution curves, indicating a complex exposure history. The surface clast exposure minimum age for Algarrobal is 0.7–1.4 Ma, substantially younger than samples from Pampas Limos and Railroad (Table 3). These are minimum exposure ages, and given the long duration of this exposure, these results are insensitive to inherited radioactive radionuclides.

Except for physical spalling, quartz fragments in this climate are not expected to be impacted by chemical weathering and significant continuous erosion. Profile dating was conducted only at the Railroad location. Due to a very low quartz content in this soil, only four samples produced sufficient quartz for <sup>10</sup>Be and <sup>21</sup>Ne analyses. To place the Railroad data into the local context, we also show the depth profiles for <sup>10</sup>Be and <sup>21</sup>Ne

for the next youngest regional landform—that is mapped as a Plio-Pleistocene alluvial deposit (Yungay)-and the CRN data for a profile excavated into a prominent active wash in the region (Fig. 4). The later two sites were reported in Jungers et al. (2013). In essence, these three profiles represent the chronosequence of Neogene alluvial landforms in this region. <sup>10</sup>Be is lowest in the wash, and much higher in the older landforms as expected, though there is only a minor difference in the amounts of 10Be in the two oldest landforms (Fig. 4A). In terms of <sup>21</sup>Ne, the concentration increases consistently with relative landform age (Fig. 4B). Attempts to model, or interpret, the depth profile via Equation 2 were unsuccessful. As discussed next, we interpret this to indicate that soil particles in these soils experience complex vertical movement over time.

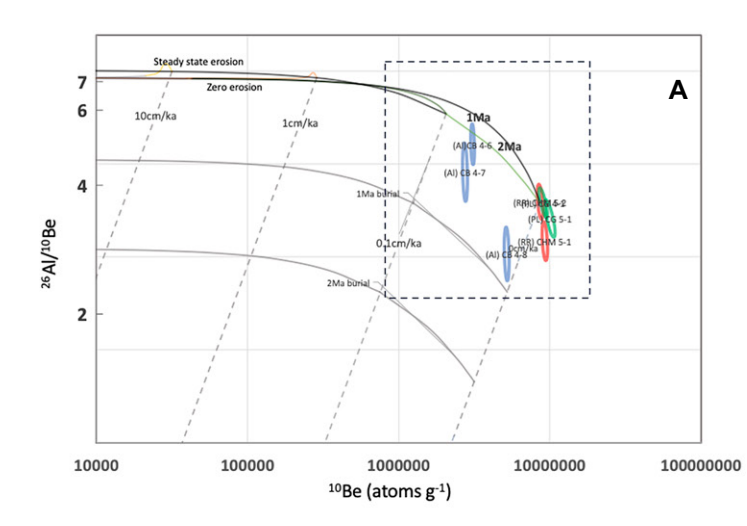
When placed on an isotope evolution diagram, it is apparent that the samples have a complex exposure history (Fig. 5). The complex history of these samples is expected in that the soils have accreted enormous amounts of salt and dust

(discussed in Elemental gains/Losses section), and have experienced considerable mixing and volumetric expansion. The depth profiles do not follow the expected exponential decline in <sup>10</sup>Be or <sup>21</sup>Ne with depth.

Two very simple exposure age calculations can be made. First, assuming the samples are exposed continuously at the soil surface with no erosion, or that they have been at the same depths continuously (with no erosion) over the duration of exposure (and, in both cases, after accounting for the inherited <sup>21</sup>Ne found in the active channel). These calculations are presented in Table 2, and while the direct linkage to absolute landform age is tenuous, the calculations do indicate very long exposures and pre-Quaternary ages for the profile, consistent with the surface clast exposure chemistry.

## Landform Ages: Discussion

Based on both surface samples and qualitative interpretations of the depth profiles, these are soils formed in landforms of considerable age, suggesting Miocene ages for the Railroad and



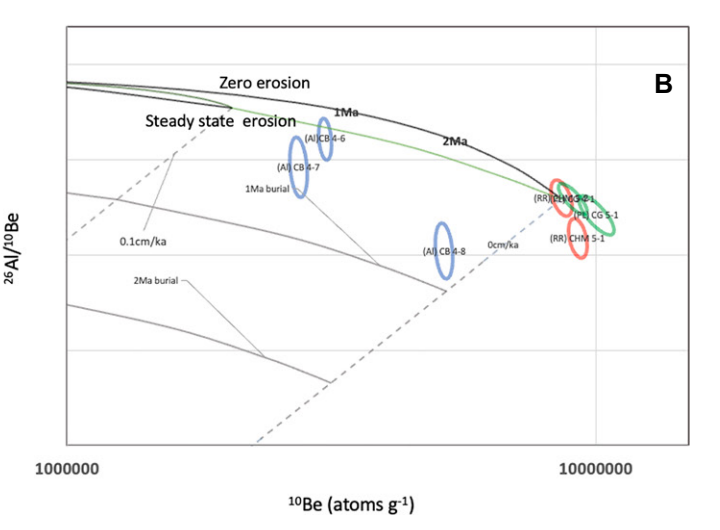


Figure 3. (A) <sup>10</sup>Be versus <sup>26</sup>Al/<sup>10</sup>Be plots for surface clasts sampled at or near each site. Samples that lie below the evolutionary line for that location (with the assumption of constant erosion) have a complex exposure history, with some burial and re-emergence suggested by the nuclide data. The ellipses illustrate the uncertainty in ratios and estimates ages (Table 3). (B) An enlargement of the boxed area in part A.

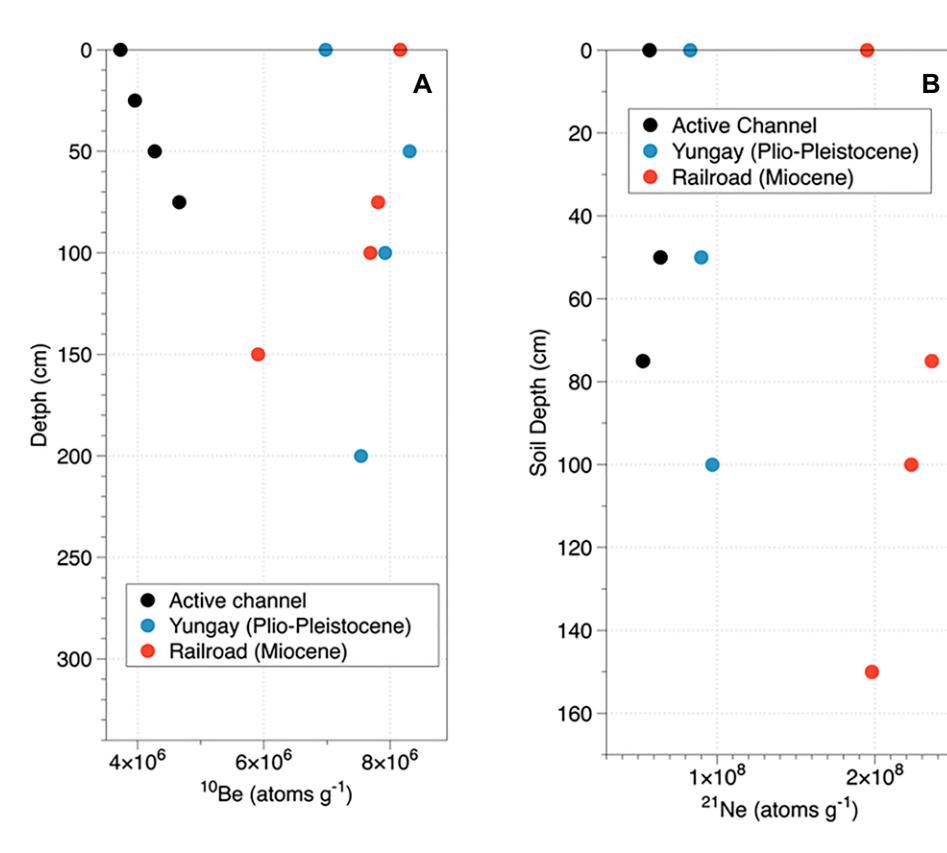


Figure 4. Published (active channel and Yungay; Jungers et al., 2013) and this work (Railroad) (A) <sup>10</sup>Be and (B) <sup>21</sup>Ne concentrations in quartz grains purified from bulk samples. All these locations are in close proximity to each other, representing a fluvial/alluvial chronosequence.

Pampas Limos sites, and at least early Pleistocene for the Algarrobal location—though given the complex history of these samples (Fig. 3), these are minimum ages. However, a deeper analysis should consider the impacts of complex physical processes over long expanses of time, especially when interpreting the observations of depth profiles, using relatively simple mathematical frameworks.

First, for the surface samples, it is interesting that the samples for the two driest locations tend to fall generally along the dual isotope evolution pathway for little erosion or burial, while the wettest site (in a biologically active climate) has evidence of complex exposure histories. The processes that form desert pavements through the accumulation of aeolian dust and salt are well known (McFadden et al., 1987), creating a lag of clasts that "float" on top of the accreting dust. Certainly, all of our sites, over their long history, have experienced climate changes, but it seems from these relatively few samples that the southernmost site has experienced the most significant biotic and/or physical disruptions of the material on the pavement over time.

Second, under simple physical conditions when a sedimentary unit is deposited, the quartz

grains within it (with some initial radionuclide content) undergo <sup>10</sup>Be, <sup>26</sup>Al, and <sup>21</sup>Ne nuclide production that declines with depth, and in the case of <sup>10</sup>Be and <sup>26</sup>Al, decay simultaneously occurs. In this case, concentrations should decline exponentially with soil depth due to attenuation of cosmic rays and decay of <sup>10</sup>Be and <sup>26</sup>Al, creating depth profiles and inventories reflecting the total exposure time of the sediment. However, the soils in the Atacama Desert have several complicating factors that affect depth profile interpretations:

- First, as will be discussed further below, the soils have accumulated enormous amounts of salt and dust, causing volumetric expansion, with a corresponding burial of some minerals, and an uplift of others (Jungers et al., 2013; Wang et al., 2015).
- Second, it is unclear if this expansion has occurred continuously or episodically. For example, Figure 2G (photo of Railroad profile) shows evidence of at least two major episodes of sulfate polygon formation.
- Third, the physical processes that create the sulfate-rich polygons may move particles upward and downward during expansion and contraction cycles, and the cracks between the

polygons serve as direct conduits for the downward movement of surficial dust (see Fig. 2G).

• Fourth, the initial cosmogenic nuclide concentration of dust and fluvial sediment is likely spatially and temporally variable, and little work has explored this issue in the Atacama Desert (Placzek et al., 2014).

Thus, no one (or simple) mathematical framework can be used to interpret the measured cosmogenic nuclide data, and the lack of a simple systematic depth trend in cosmogenic nuclide is to be expected. This is especially relevant for the very complex Railroad soil examined here, which lacks systematic <sup>10</sup>Be and <sup>21</sup>Ne behavior with depth.

One very simple way to interpret the <sup>21</sup>Ne data is to subtract the initial inheritance and use the remaining <sup>21</sup>Ne as a simple guide of overall inheritance. The active stream channel quartz grains themselves contain enough <sup>21</sup>Ne to represent 2.3 m.y. of surficial exposure. After subtracting this from the Railroad samples, the <sup>21</sup>Ne "ages" for the Pampa de Mulas formation (Railroad site) are consistent with the geological mapping and with exposure ages of the surface samples (Table 2).

# **Pedogenic Alteration Patterns**

### Elemental Gains/Losses: Results

The total elemental concentrations of fines and gravels are provided in the Supplemental Material (Table S11). The mass gains/losses were calculated using Equation 3, which requires an immobile reference/index element. An ideal index element (Equation 3) must be (1) chemically inert and (2) evenly distributed throughout the parent material. Ti and Zr are common choices in, for example, granitic terrain but tend to be concentrated in heavy minerals and thus are subject to physical winnowing during fluvial transport and deposition. For the Algarrobal location, Ebeling et al. (2016) found erratic relations between Ti and Zr, which also extend to all the soils in aggregate here (Fig. 6B). In the gravel fraction (>2 mm) of the soils, which should reflect the lithology of the source area, two elements that are candidate index elements should have a constant elemental ratio. In this study, Ti versus Zr is not constant. This could be due to either (or both) Ti and Zr violating either of the constraints above. It has been suggested that rare earth elements (REE) are more evenly distributed in minerals of all densities (Gromet

<sup>&</sup>lt;sup>1</sup>Supplemental Material. Total geochemical analyses of the soils examined. Please visit https://doi.org/10.1130/GSAB.S.26142322 to access the supplemental material; contact editing@geosociety.org with any questions.

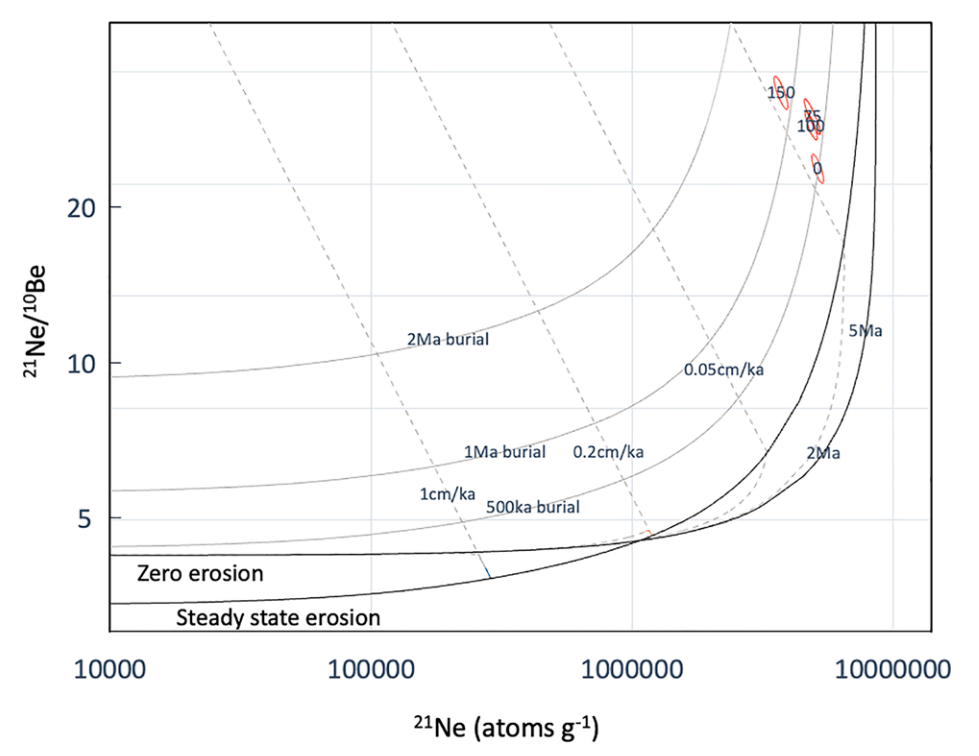


Figure 5. The relationship between <sup>21</sup>Ne/<sup>10</sup>Be versus <sup>21</sup>Ne as a function of time, steady-state erosion, and burial. The four samples from the Railroad soil are illustrated within this framework.

and Silver, 1983), which may assist them in circumventing differential winnowing of minerals during transport. Ti versus Zr, and Ti (and Zr) versus Ce or Nd produced non-constant ratios. We conclude that both Ti and Zr have erratic behaviors due to physical sorting of heavy minerals during fluvial transport (Fig. 6B) and that Ce and Nd both are relatively evenly distributed and immobile (Fig. 6A). As discussed in the following section, REE are also subject to apparent chemical weathering processes. Thus, while we identify no perfect index element, the REEs

in general, and Ce used here and elsewhere (Ebeling et al., 2016), are good first-order constraints on major elemental changes with depth and space.

The gains/losses of common rock forming elements in the profiles are illustrated in Figure 7. The apparent magnitude of loss declines with increasing northerly latitude consistent with trends in Ewing et al. (2006) for Plio-Pleistocene-aged soils. The Algarrobal soil has losses of Si, Al, Fe, Mg, K, and P in the upper 2 m. The Pampas Limos soil shows both some evidence of

subsurface losses of the rock-forming elements, and some near-surface gains. It is important to note that relatively less-weathered dust influx likely mutes previous elemental losses in all the soils and contributes to some of the apparent gains of elements in the driest sites. In contrast to the other sites, the Railroad soil reveals little evidence of significant chemical depletion of the rock-forming elements and some apparent significant gains.

The gains/losses of REEs also follow some of the latitudinal trends of the major rock-forming elements. On a very broad level, there is a decrease in the deviation of REE tau values, relative to gravel, with decreasing rainfall (Figs. 8A–8C). The deviations from parent material values also tended to decline with depth.

Elements associated with salt and dust inputs (Ca, Na, S, and C [total C by Leco furnace]) are considered last. In general, relative gains of Ca, Na, S, and C (total) increased with increasing aridity (Fig. 9). The one major deviation from this trend was total C, which had the largest overall increase in the Algarrobal soil (which has large quantities of pedogenic carbonate: Ebeling et al., 2016).

Total sulfate isotope trends with depth mirror that of the sulfate depth patterns (Fig. 10). In general, the  $\delta^{34}$ S and  $\delta^{18}$ O values of the sulfate decline with depth, and the  $\delta^{34}$ S of total S declines with depth, reflecting observed patterns caused by isotope fractionation as sulfate undergoes dissolution/reprecipitation during downward transport (Ewing et al., 2008a; Amundson et al., 2012b).

## Elemental Gains/Losses: Discussion

There are two major trends, and implications, of the elemental results presented in the previous paragraphs. The first is the obvious chemical verification that the soils have accumulated significant amounts of dust and salt (Fig. 9), in

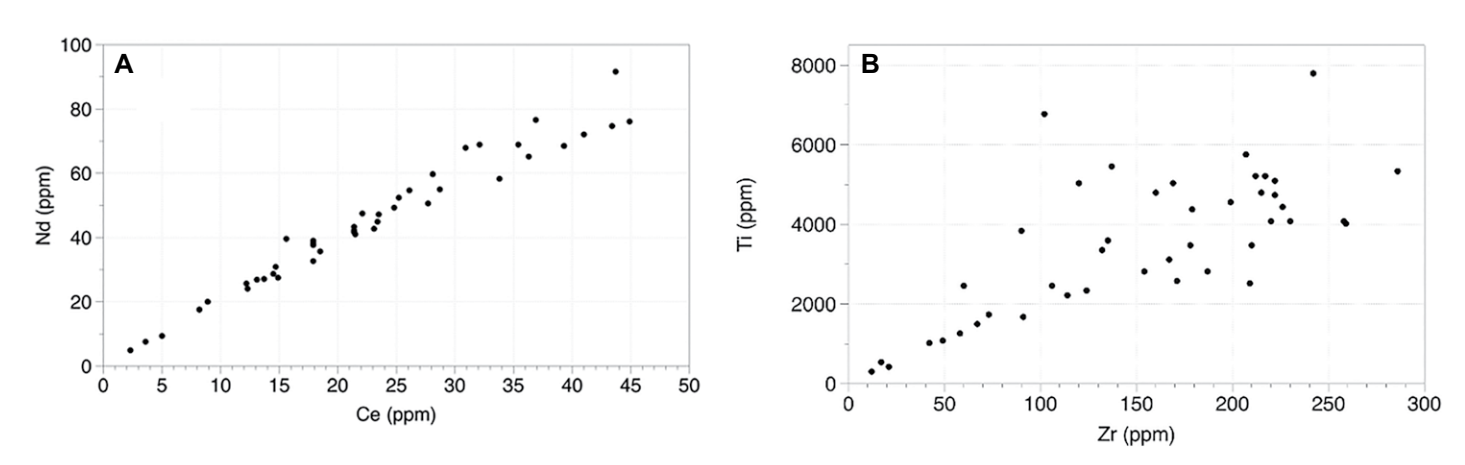


Figure 6. Correlation between (A) Ce and Nd and (B) Zr and Ti for the <2 mm fraction and selected gravel fractions for the three soils examined here.

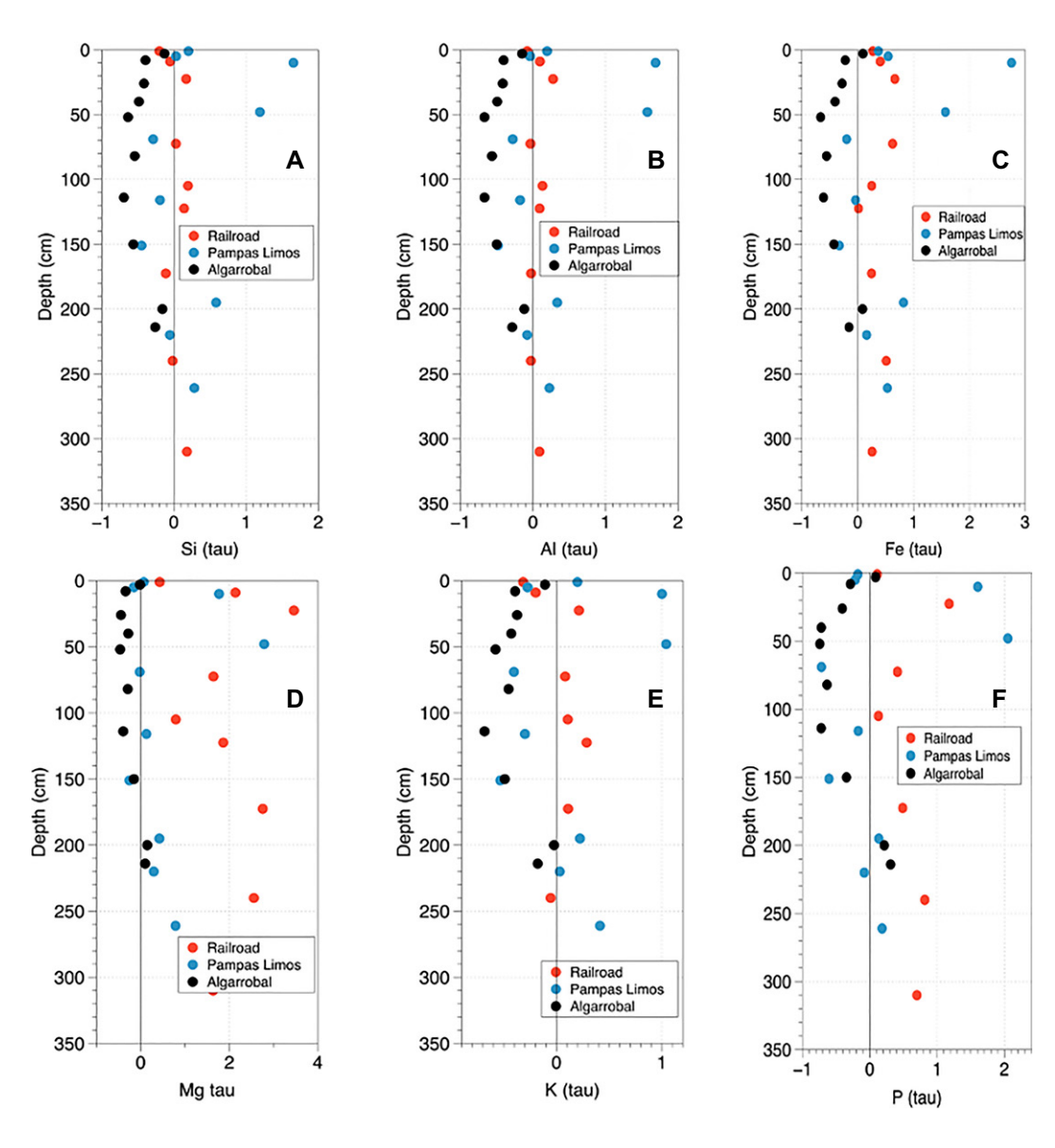


Figure 7. Tau values versus soil depth for the rock-forming elements (A) Si, (B) Al, (C) Fe, (D) Mg, (E) K, and (F) P. Values less than 0 represent fractional losses; values greater than 0 represent fractional gains relative to parent material.

amounts and patterns generally consistent with their present climate conditions and regional soil forming conditions. Sulfates and chlorides (reflected by the high relative Na gains) accumulate in the driest soil (Railroad; Figs. 9B and 9C). Sulfates appear in the largest accumulation in the Pampas Limos soil (Fig. 9C), while carbonate (as total C) is the largest gain in the southernmost locale (Algarrobal; Fig. 9D).

The second major finding is that the soils have experienced losses of some rock-forming elements and REEs (Figs. 7 and 8) that follow a latitudinal trend: largest losses in the southernmost soil and negligible losses at the northern Railroad location.

These two different trends, loss of rock-forming elements (Fig. 7) and gains of more soluble components (Fig. 9), are chemically incompatible, and the processes that produced the trends must therefore be separated in time. Addition-

ally, the conditions inducing the losses must have occurred prior to the conditions driving the gains. This was the conclusion of the earlier analysis of the Algarrobal soil (Ebeling et al., 2016), but the work here extends this along a significant climate/latitudinal gradient.

While the use of index elements to estimate elemental gains and losses is a powerful interpretive tool, it is subject to complications. The most important here is the influx of dust and aerosols that have unique elemental compositions relative to the alluvium. Relatively less-weathered dust influx thus may likely mute actual elemental losses in all the soils. In field notes made during sample collection, we noted significant weathering and grusification of granitic gravels in both the Pampas Limos and Algarrobal profiles. No significant clast weathering was observed in the Railroad profile. While today the Pampas Limos soil has an approximate rainfall similar to the

Railroad site, as discussed in the following paragraphs, there are significant differences in chemical weathering, suggesting locally different climatic histories for these northernmost sites.

The depth and latitudinal trends of REEs reinforce the interpretation of some "early stage" aqueous weathering of the soils, a trend of alteration that appears to decline with northerly latitude. The behavior of the REEs (the Lanthanides plus Y) during soil weathering has not been explored as deeply as major element behavior, but some insights into differential behavior of the REEs have been examined through normalization to chondrite value (e.g., Minařík et al., 1998; dos Santos et al., 2019). While this normalization provides insights into REE behavior versus depth or climate, it does not provide information on quantitative mass gains or losses relative to the parent material. It is sometimes assumed that, due to their similar charge and

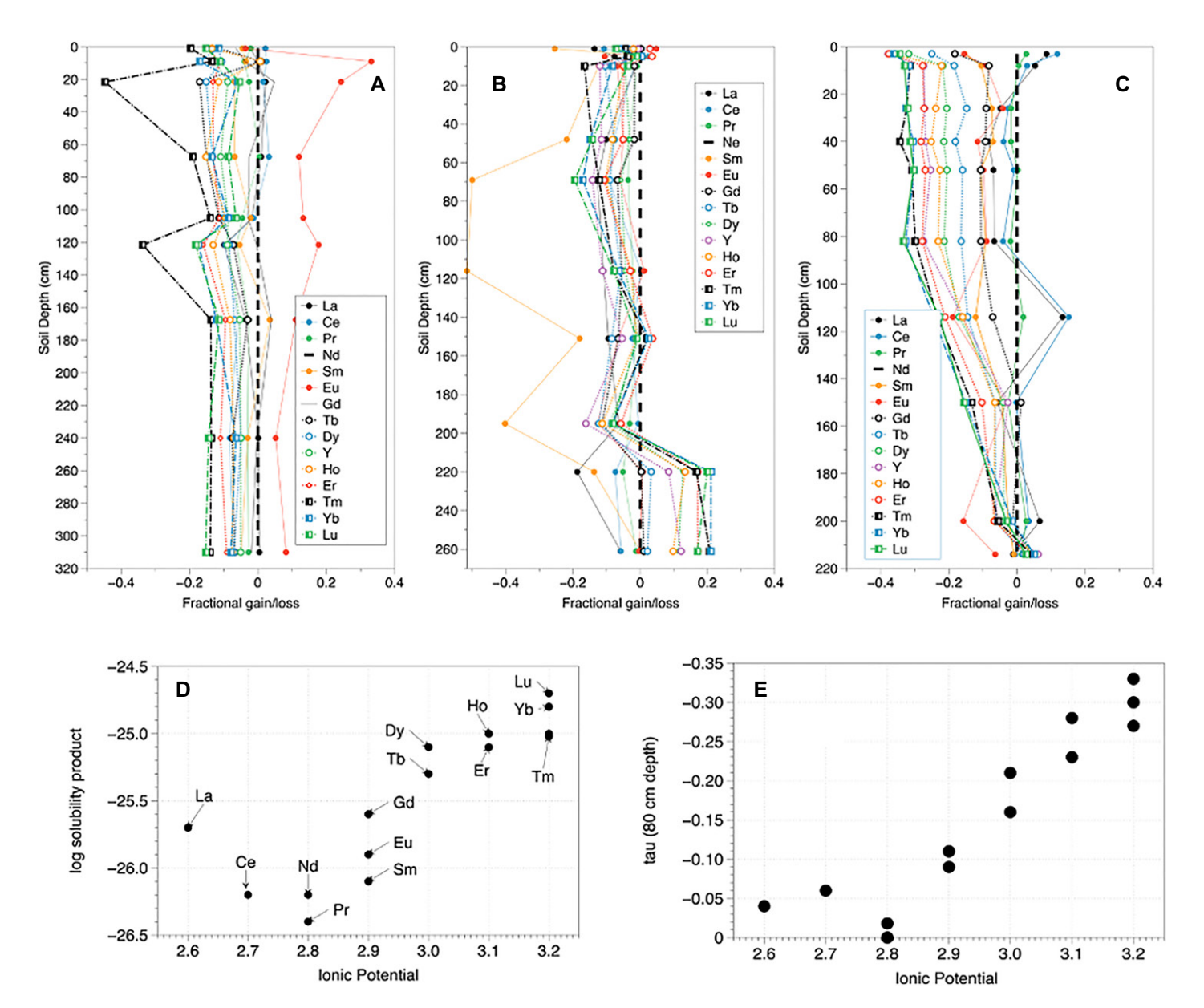


Figure 8. Rare earth element (REE) gains/losses relative to Nd and local fresh gravel for the (A) Railroad, (B) Pampas Limos, and (C) Algarrobal sites. (D) The log of the solubility product of REE phosphate minerals (data from Cetiner et al., 2005) versus REE ionic potential and (E) the tau values for REE from 80 cm in part A versus ionic potential.

radius, REEs behave similarly in soil environments. Indeed, we have found similar relations between Ce and Nd, which led to our choice of a reference element to calculate gains or losses.

However, there are differences in ionic potential among these elements, which helps determine elemental solubility in natural waters (Railsback, 2003). Additionally, there is a growing interest in the solubility of REE with different anions in natural waters. The log of the solubility product of REE phosphates (Cetiner et al., 2005) versus REE ionic potential (which increases with atomic number) is shown in Figure 8D, which suggests increasing solubility with

increasing ionic potential for the REEs. One of the few, and earliest, approaches to examining the fate of REEs during soil weathering using the tau approach is that of Nesbitt (1979). Nesbitt used Ti as an immobile element in examining REE element behavior in the weathering of granitic core stones in soils. Here, we used Nd as an index element and the REE/Nd content of fresh gravels in each site as the unweathered reference (Figs. 8A–8C). The choice of Nd was arbitrary, though based on its low solubility (Fig. 8D), and similar patterns would emerge if Ce was used. The Algarrobal soil, which reveals significant REE losses, has patterns of relative loss (tau val-

ues) that generally mirror the trends of solubility versus ionic potential (Fig. 8E), revealing that their behavior is not identical, and predictable from their atomic characteristics.

Three very pronounced REE deviations were observed: (1) a Sm depletion at Pampas Limos, (2) a Tm depletion, and (3) a Eu enrichment at the Railroad site (Fig. 11). All three of these are likely signatures caused by dust inputs, which are either enriched or depleted in these select elements relative to the gravels. The depth trends of these enrichments/depletions correspond to zones of salt and visible dust accumulation (Fig. 2). This analysis reveals

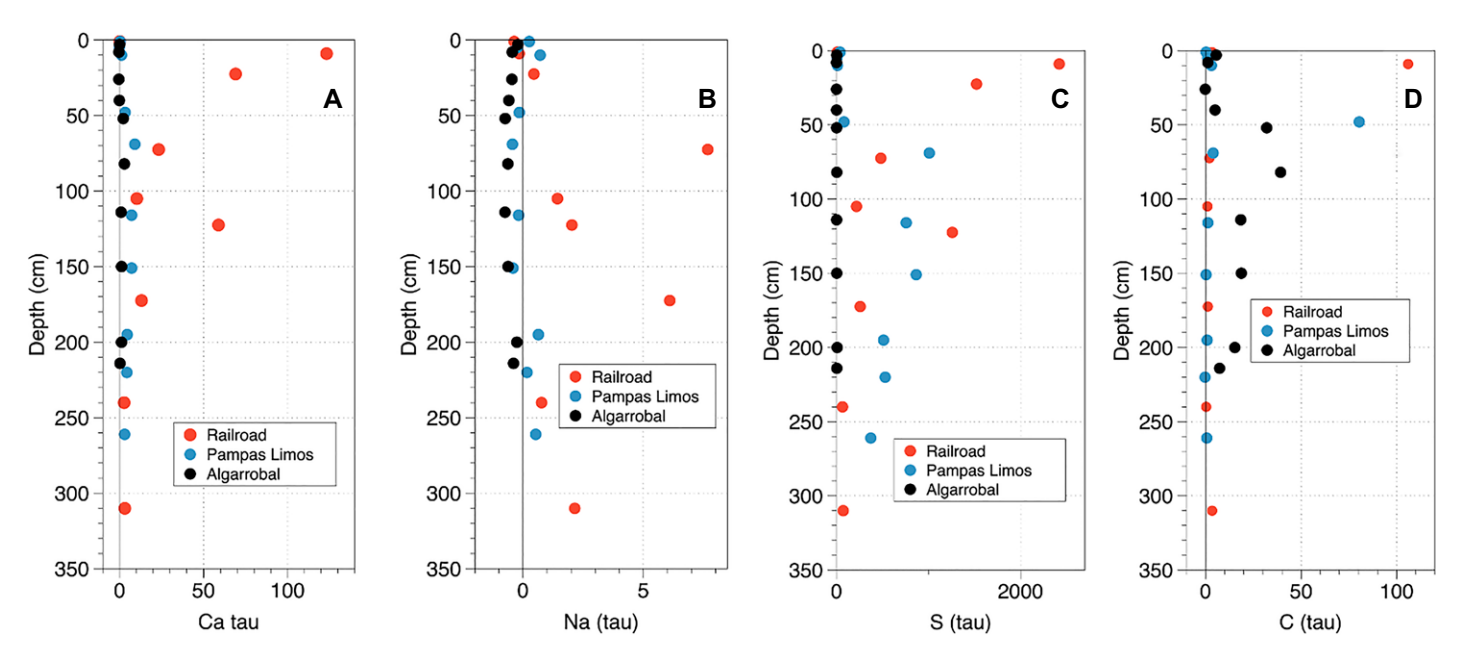


Figure 9. Tau values (relative gains/losses versus fresh gravel) for (A) Ca, (B), Na, (C) S, and (D) C for the three soils.

local chemical tracers that can be exploited to quantify dust and aerosol accumulations. We have only one dust sample on which we have REE geochemistry data: the Yungay site a few kilometers to the west of the Railroad site examined here. In this sample (Table S1), there is no apparent Eu or Tm anomaly relative to the parent material REE values at the Railroad site. We note, however, that the present dust chem-

istry bears a strong enrichment of Cs, Cu, Mo, Pb, and Sn relative to soils or gravels, reflecting significant anthropogenic Cu-ore processing influences on present deposition. Thus, at this stage, we can only offer hypotheses for the trends in Figure 11.

Sulfur enrichment increases with decreasing rainfall, and is most prevalent in the upper 2 m of the soils (Fig. 9C). The mineralogical com-

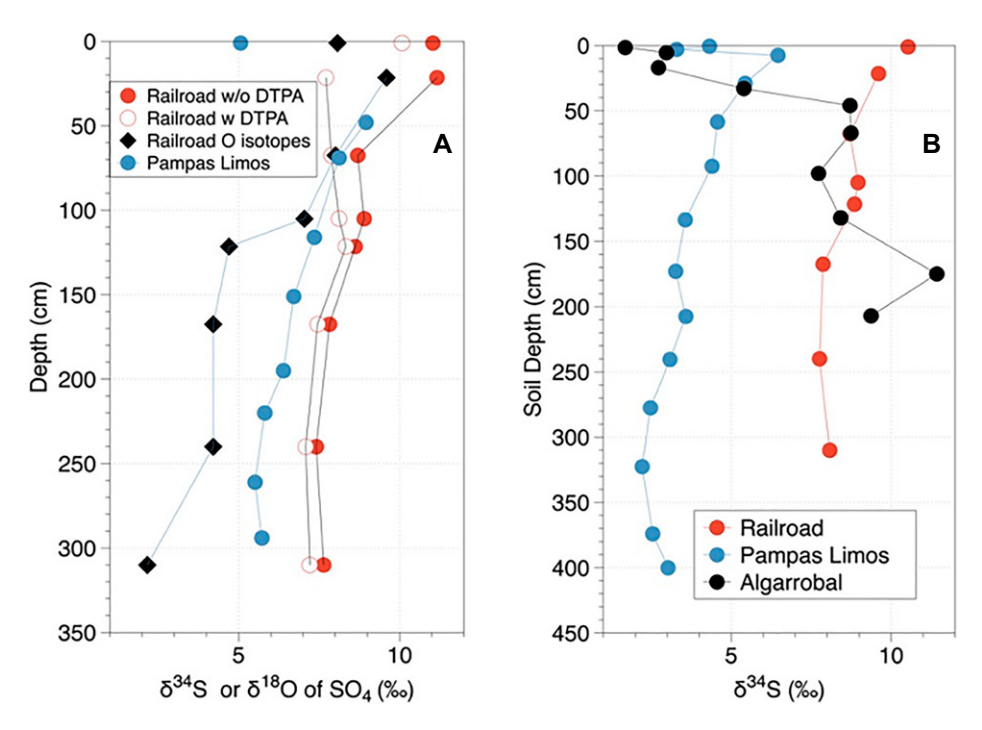


Figure 10. (A)  $^{34}$ S and  $^{18}$ O values for sulfate from the Railroad and Pampas Limos soils and (B)  $^{34}$ S values for total S from all three soils. DTPA—diethylenetriamine pentaacetate.

position is likely a mixture of gypsum and anhydrite (Ewing et al., 2006; Pfeiffer et al., 2021). In the two most arid soils, S tau is linearly correlated with Ca tau, reflecting the sulfate mineralogy (Fig. 12A). At the wettest site, C tau is correlated with Ca, reflecting the accumulation of CaCO<sub>3</sub> from external sources. There is a very small amount of carbonate in the Pampas Limos soil, with some associated Ca (Fig. 12B). Na tau enrichments are greatest in the Railroad soil, and there are small enrichments at depth at Pampas Limos (Fig. 9B). The Na tau enrichments generally are deeper in the soils than the Ca enrichments, reflecting the higher solubility of common Na-bearing minerals (halite, nitratine, Na<sub>2</sub>SO<sub>4</sub>) versus Ca-bearing minerals (gypsum, anhydrite). The total geochemical analyses did not include Cl (but was measured in Amundson et al., 2012b, for the Railroad site), but Na has no strong relationship with S, suggesting most of the Na addition is present in the form of NaCl, which was both visible and detectable by taste.

The depth trends in S and  $SO_4$  isotope composition reflect the patterns and mechanisms discovered by Ewing et al. (2008a) and further expanded by Amundson et al. (2012b; see also Fig. 10). Briefly, incoming atmospheric sulfate can be derived from sea salt ( $\delta^{34}S = 21\%$ ), marine biogenic emissions (13%–20%), or rock/salar derived sources ( $\pm 5\%$ ). Sulfate from both the Railroad and the Pampas Limos sites are skewed toward rock/salar inputs, but overall, the  $\delta^{34}S$  value of the Railroad site is  $\sim 4\%$ 0 greater (Fig. 10A). The fact that the Railroad site is at the upper limit of the fog belt suggests

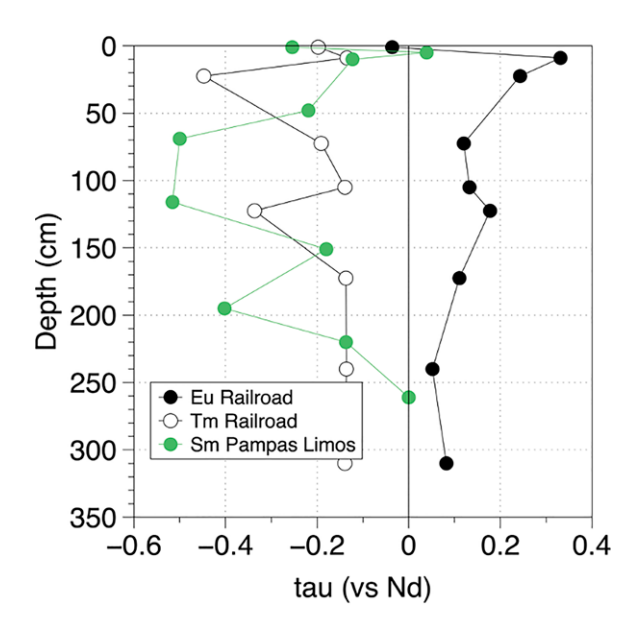


Figure 11. Depth profiles of selected rare earth element tau values reflecting exogenous dust inputs.

there is some input of marine S sources, likely contributing to the slightly higher  $\delta^{34}S$  values. The Pampas Limos site, due to its high elevation, should receive largely redistributed salts from rock outcrops and salars. Once sulfate is deposited, it is steadily winnowed downward by rare rainfall events of varying magnitude—over long expanses of time. This slow process of mineral dissolution and reprecipitation favors the retention of heavy isotopes of S and O near the surface, and the preferential movement of  $^{34}S$  and  $^{18}O$ -depleted  $SO_4$  to greater depths. The Railroad and Pampas Limos sites clearly reflect these processes (Fig. 10A). The fact that signifi-

cant accumulations occur to depths greater than 2.5 m indicates that rare rainfalls must be large enough to dissolve and move solutes deeply. However, as discussed below, the fact that the soils are also volumetrically expanding magnifies the apparent depth of water movement.

At the Railroad site, total S and  $SO_4$   $\delta^{34}S$  trends with depth are approximately the same, since total S is expected to be nearly entirely  $SO_4$  (Fig. 10). At the Pampas Limos site, total S is  $\sim 2\%$ –2.5%0 depleted relative to  $SO_4$ . This is interpreted to reflect some S from possible biotic sources, which are likely to be more depleted in  $^{34}S$  (Yi-Balan et al., 2014). It is

possible that some of this hypothetical organic S remains from brief, more pluvial, interludes. In the Algarrobal soil, the surface has the lowest  $\delta^{34}$ S value of all the soils, and the  $\delta^{34}$ S increases steadily with depth, to the highest value (>11‰) observed along the transect. We interpret this to represent the imprint of the increasing importance of biology at this location. A very cursory explanation is that isotopically light S is preferentially used in biological processes, and remaining  $^{34}$ S-enriched sulfate (albeit in very low concentrations) is moved downward out of the surficial zone of intermittent biological activity.

#### CLIMATE IMPLICATIONS

# Pace and Pattern of Landscape Evolution

The soils examined began forming sometime in the very late Miocene or, for the southernmost site, possibly the Pliocene. For some extended interval, the soils were exposed to climates that drove either minor chemical weathering (Railroad in the north) or caused significant chemical weathering and loss of rock forming elements that cannot occur under current dry climate conditions (e.g., Pampas Limos and Algarrobal to the south). The early post-depositional phase that impacted these sites occurred during a time when the Pacific is proposed to have been set in a permanent El Niño, or a situation also called the "El Padre" pattern (Ford et al., 2015; Wara et al., 2005; see also Fig. 13), which today accentuates rainfall incursions into the southern Atacama Desert during the austral winter

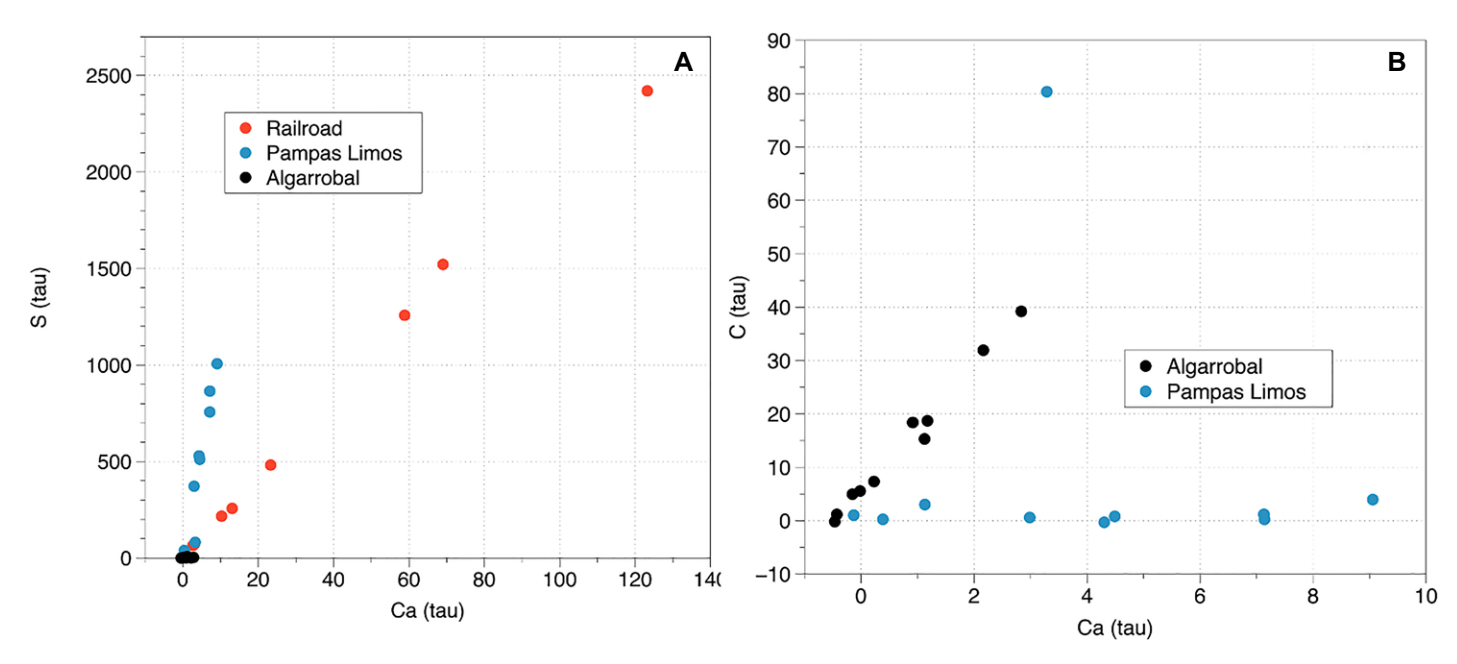


Figure 12. (A) Correlation between Ca and S tau values and (B) Ca versus C tau values for the soils.

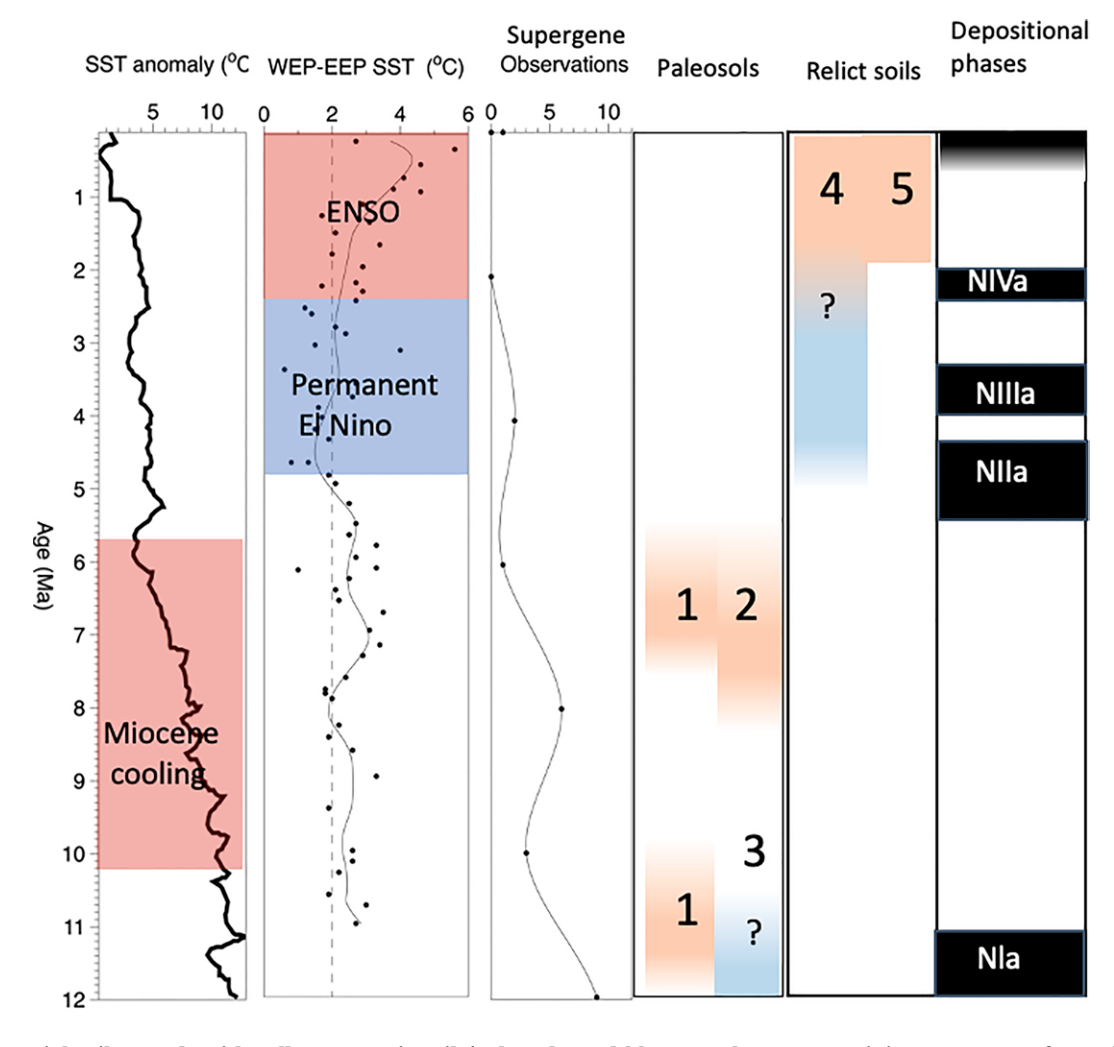


Figure 13. Southern Pacific sea surface temperature (SST) anomalies (relative to present temperature) from 12 Ma to the present for compiled cores between 30°S and 50°S (extracted from fig. 3a in Herbert et al., 2016). The difference in western equatorial Pacific (WEP) versus eastern equatorial Pacific (EEP) SST over time, calculated by subtracting SST at site 850 from site 806 using data from Zhang et al. (2014). The pink box for Miocene cooling is expanded from Herbert et al. (2016), and the blue box for the El Padre "permanent El Niño" is time frame reported in Ford et al. (2015). A compilation of radiometric ages for minerals associated with supergene copper enrichment in the Atacama region. The diagram is modeled after Vasconcelos et al. (2015), with data from Alpers and Brimhall (1988); Bouzari and Clark (2002); Marsh et al. (1997); Mote et al. (2001); Arancibia et al. (2006); and Sillitoe and McKee (1996). Data binned by 2 m.y. segments, with the youngest number of the segment used for data point. Paleosol and surfi-

cial soil records with yellow = gypsic soils/paleosols, and blue = carbonate containing or gypsum free soils/paleosols. Paleosol data from Rech et al. (2019) and ages provided in their supplementary data. Major depositional events from Jordan et al. (2014) are ranges reported for regional incision events in pediplains in the northern Atacama desert. ENSO—El Niño—Southern Oscillation.

(Houston, 2006). Given the degree of elemental loss in the soils, there was adequate rainfall in at least the southernmost location to support significant vegetative cover and enough water to prevent the accumulation of most salts. The sediments themselves would have undergone volumetric expansion due to roots and additions of organic matter, which was countered by mass loss and associated volumetric collapse. In all the soils, the estimated loss of major elements is likely partially countered by the addition of less-weathered (relative to gravel parent material) dust. The REEs suggest that REE chemistry of the dust endmember might constrain dust inputs, but we do not have adequate data. All that REE can say without the dust endmember is that significant fractions of the soils are from exogenous sources (Fig. 11). What is striking is that the apparent chemical "intensity" of this early more pluvial phase decreased significantly

with decreasing latitude. The southernmost soil has visually weathered cobbles and gravels and significant amounts of pedogenic clay, while the northernmost soil appears to have largely unweathered clasts and little evidence of significant silicate weathering. This suggests a much sharper gradient in rainfall with latitude than that which exists today.

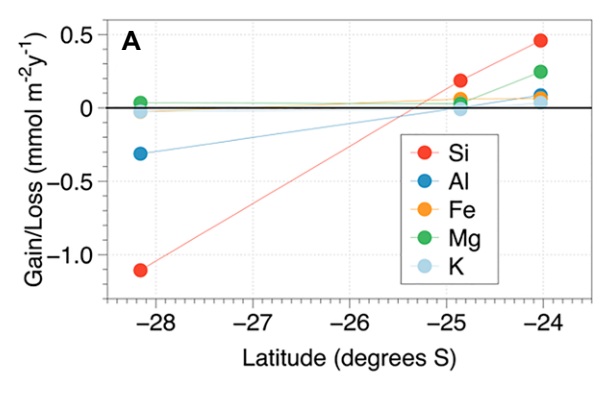
A minimum assessment of the net volumetric change of the soils can be determined by calculating the epsilon value of the soils and then calculating the fractional change in volume (Brimhall and Dietrich, 1987):

$$\varepsilon = \frac{\rho_p C_{i,p}}{\rho_s C_{i,s}} - 1 = \frac{V_s}{V_p} - 1,$$
 (4)

where  $\varepsilon$  = epsilon or volume change, C = elemental concentration, V = volume,  $\rho$  = bulk density, s = soil, p = parent material, and

*i* = immobile index element. Bulk density was measured by coring soil horizons with a percussion sampler. From this relationship, the measured profiles have vertically expanded 36 cm, 137 cm, and 167 cm from south to north since the cessation of fluvial deposition. This calculated expansion, based on Ce concentrations, matches field observations, including Zr based estimates of a doubling of overall Plio-Pleistocene soil depth in Ewing et al. (2006). For example, much of the upper 1 m of the Railroad soil lacks visible gravel, consistent with the influx of nearly 2 m of net expansion (Fig. 2G). This expansion is a unique regional landscape process.

Summing the apparent gains/losses of some rock-forming elements for the entire profile, there is a systematic increase in the loss, and rate of loss, with increasing southern latitude (Fig. 14A). As discussed, dust additions have likely masked some of a previous chemical



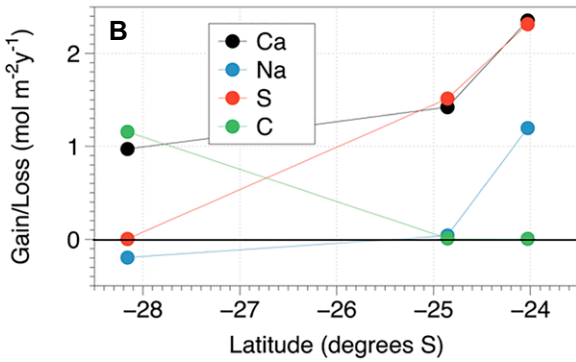


Figure 14. (A) Estimated rates of mass change of rock forming elements and (B) elements associated with salts versus latitude. Assumed landscape ages are 5 Ma for Railroad and Pampas Limos and 2 Ma for Algarrobal.

weathering loss. At the southernmost site, losses of Si and Al overwhelm any later aeolian additions, with losses of up to 1 mmol  $m^{-2}$   $y^{-1}$  Si.

The deposition of aerosols and dust over the past few millions of years have driven element gains that differ with latitude and climate. At the southernmost locality, carbonate (reflected in both C and Ca) has been accumulating at a rate comparable to Si loss (1 mmol m<sup>-2</sup> y<sup>-1</sup>). At Pampas Limos, sulfate accumulation (as Ca and S) dominates, while the Railroad site has both significant accumulations of sulfate and chloride (and likely nitrate), at rates (sulfate) of 2 mmol m<sup>-2</sup>y<sup>-1</sup>. The calculated rate for the Railroad site, based on a soil age of 5 Ma, is about the same rate as that calculated for the nearby Plio-Pleistocene aged Yungay soil (1.4 mmol sulfate m-2y-1). It is important to note that mass accumulations, and rates, have very large uncertainties. Gravel content and bulk density have enormous impacts on inventory calculations, and (especially gravel) are hard to quantify. Second, rates hinge on uncertain age estimates. That said, the relative differences between the locations are important to ascertain broad constraints on the rates of these processes.

There are likely to have been significant breaks or thresholds in these processes over time. For example, all sites show evidence that present (Holocene) conditions and processes are more arid than those that existed in the recent past (e.g., 10<sup>3</sup>–10<sup>4</sup> y). As discussed by Ebeling et al. (2016), the prevailing rainfall conditions

around Algarrobal are presently too arid for promoting massive, and deep, pedogenic carbonate accumulation. This is also consistent with carbonate accumulation observed by Ewing et al. (2006) near Copiapo, interpreted to reflect intermittent wet periods. At Pampas Limos, while we have spent less observational time in this location, the tops of the massive sulfate polygons have easily discernable dissolution pits (overlain by subsequently deposited dust and very low-density sulfate crystals) indicative of recent pluvial episodes (Fig. 2E). To the south near Diego de Almagro, Pfeiffer et al. (2021) found that pedogenic carbonate ceased accumulating in a hillslope soil near the end of the Pleistocene (and then entered a sulfate accumulation phase), which is supportive of our interpretation of the Pampas Limos site. Finally, the Railroad location (and the Pampas de Mulas more broadly) have near-surface horizontal piping systems that lie on top of the dense sulfate polygons (Amundson et al., 2012a; Pfeiffer et al., 2021). This piping system has occasional surface entry portals that show clear evidence of water expulsion and ponding following the 2015 rainfalls that occurred in the region (Pfeiffer et al., 2021).

Thus, chemical and physical evolution of these landscapes continues, with imprints of more recent processes being overlain on soils of vast age and considerable geochemical information. While the integrated record is thus complex, the continuous and long record of these relict soils make them an underutilized tool in understanding the landscape evolution of this region.

#### Paleoclimate

Research in the past decade or more has compiled much information that can be aggregated into a holistic and interesting new view of the post-mid-Miocene climate of the Atacama Desert (Fig. 13). This figure can be compared to figure 10 in Muñoz-Farías et al. (2023), who compiled evidence relative to climate at the latitude of 26°S to 28°S, which lies within the transect examined here. The next section focuses largely on the soil and alluvial record, but also includes a compilation of dates of minerals found in supergene enrichments of copper deposits in northern Chile (Fig. 13). This record is similar to that compiled by Vasconcelos et al. (2015; their fig. 3). As those authors noted, there is a peak of apparent supergene weathering and enrichment between 25 Ma and 15 Ma. From 12 Ma to 0 Ma (the focus of the landforms and soils), there is a decline (with some apparent peaks) after 12 Ma, and a near cessation of observations after 4 Ma (note: the data are binned in 2 m.y. segments, with the youngest age of the bin represented on the figure). As discussed in the following paragraphs, this framework and timeline generally corresponds to the soil and alluvial landform evolution over the same time interval.

Mid to late Miocene. Oerter et al. (2016) examined a sequence of paleosols in the mid(?) Miocene to 9.25 Ma Arrieros gravels (the ages refined by Fernández-Mort et al., 2018) in the El Tesoro open pit copper mine south of Calama. These soils showed climate oscillations from subhumid (Fe oxidation and no carbonate) to semiarid (carbonate accumulation) throughout this thick stratigraphic section of fluvial gravels. The soils contained evidence of burrowing animals, and thus biotic conditions far different than the abiotic desert that exists today. There was no evidence of hyperarid conditions within this sedimentary record.

Rech et al. (2006, 2019) and Hartley and May (1998) have examined a number of paleosols embedded in sedimentary deposits. The recent work by Rech et al. (2019) show that these paleosols extend from 19°S to 26°S—the entire length of the present Atacama Desert. Lower middle Miocene soils (24–14 Ma) are calcareous, and have evidence of roots, consistent with observations of Oerter et al. (2016) and with the abundant evidence of supergene enrichment of copper (Fig. 13). However, upper middle Miocene paleosols (10–8.3 Ma) have enormous quantities of gypsum, indicative of hyperarid conditions. Similar soils are found in eolian deposits bounded by ashes 8.5 Ma and 5.5 Ma

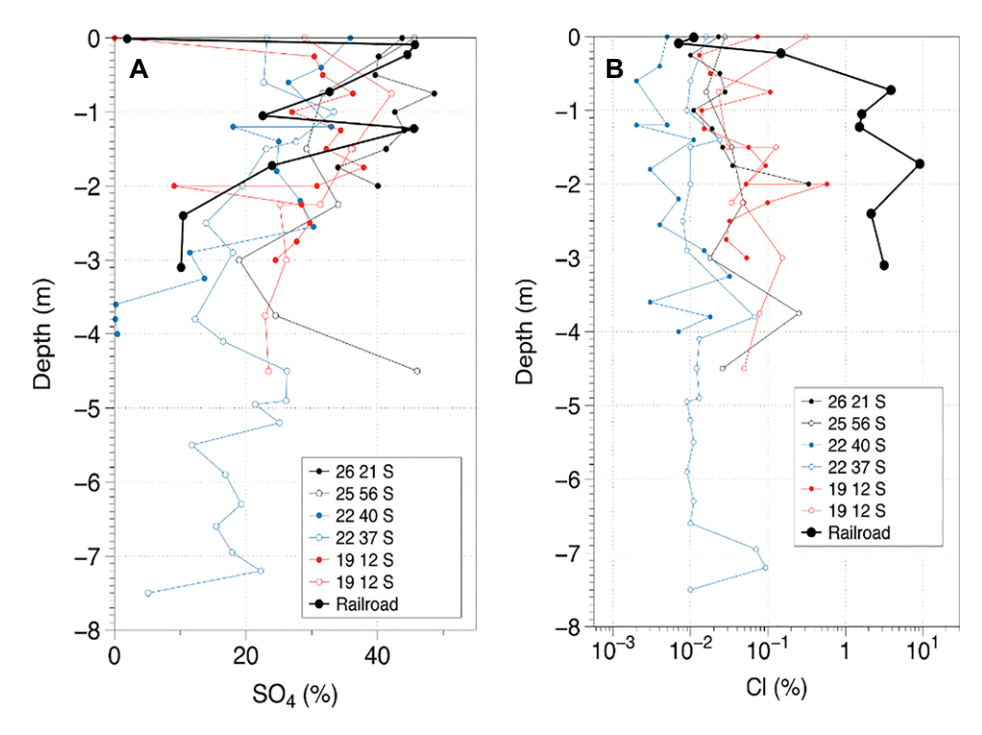


Figure 15. (A) Sulfate concentration of Miocene paleosols and the Railroad soil and (B) Cl content of the same soils. Paleosol data from Rech et al. (2019).

(Blanco and Tomlinson, 2013). These regionally distributed gypsic paleosols are geochemically similar to the relict Railroad soil examined here, though the depth of sulfate accumulations tends to be deeper in a number of locations (Fig. 15A). The interpretation that the paleosols experienced millions of years of soil development before burial (Rech et al., 2019) seems reasonable when compared with surface soils of today. As Rech et al. (2019) also noted, the Miocene paleosols have a very low Cl content, particularly when compared to the Railroad soil (Fig. 15B) and the nearby Plio-Pleistocene Yungay soil (Ewing et al., 2006). Both the depth of the sulfate penetration and the lack of NaCl suggest slightly more humid conditions than those which presently occur in the hyperarid desert.

Latest Miocene to present. The regional late Miocene gypsic buried soils have been buried by a combination of ignimbrites and fluvial sediments (e.g., Muñoz-Farías et al., 2023). The fluvial sediments indicate a rejuvenation of erosional processes, and presumably increased rainfall. Additionally, all of these Miocene deposits are impacted by extensive later incision, forming an extensive inset of late Pliocene to earliest Pleistocene landscape that is prominent in many locations (Amundson et al., 2012a). Our interpretation is similar to that of Jordan et al. (2014), whose work focused on the northern Atacama desert, north of Calama. It also is in line with the observations of Muñoz-

Farías et al. (2023), who found that Atacama Pediplain deposition ceased between 5.2 Ma and 3.8 Ma. However, at that location, incision of the Miocene sediments is attributed to a combination of uplift and stream capture.

While there are presently differing controls or sources of rainfall in the northernmost Atacama (moisture from the east) versus the southern (Pacific moisture) Atacama, there appears to be some broad similarities of the timing of less arid episodes, periods that correspond to either stability of Pacific sea surface temperatures (SST) or periods of increasing SSTs (Fig. 13). These events must have been driven more by rainfall and water than presently exists, and much of it was likely derived from the mountains upslope. However, the fact that regional hillslopes around the Railroad location suffered the loss of silicate soils around this time suggests some meteoric waters and surficial processes at least temporarily were active in what is now the hyperarid desert (Amundson et al., 2012a; Owen et al., 2011). In line with these observations, the Railroad soil has two distinctive levels of sulfate polygon formation (Fig. 2G) that suggests an interruption in hyperarid conditions during its exposure history. Since the Pliocene, it appears all regions were locked into roughly two million years (post Pliocene) of aridity somewhat similar to that of today.

Atacama climate and SST. A growing understanding of global sea temperatures and their

geographical patterns is emerging that appears to provide a possible first-order framework for the observed sequence of soil chemistry and fluvial activity in the Atacama Desert. The present climate system, driven by a strong meridional SST gradient and cool surface waters in mid latitudes, produces a strong Hadley cell system of descending warm dry air in latitudes near the Atacama, an ocean-climate pattern that began to establish itself at the end of the Pliocene (Brierley et al., 2009; Fig. 13).

SSTs during the early- to mid-Miocene were 6 °C warmer than today (Lear et al., 2000) (Fig. 13). This resulted in small differences between equatorial and mid latitude SST, weakened the Hadley circulation, and greatly increased rainfall in what are now arid regions (Herbert et al., 2016). In both deep-sea-derived and sea-surface-derived proxies, a protracted cooling episode began after 12 Ma (Lear et al., 2000; Herbert et al., 2016) that contracted and strengthened Hadley cells and corresponded to global increases in aridification in Africa and Asia (Herbert et al., 2016).

During the Pliocene, SSTs stabilized, and the meridional gradient between tropical and southerly latitudes again declined (Ford et al., 2015). This is projected to have again increased rainfall during the Pliocene in northern Chile by roughly an order of magnitude relative today (fig. 3 in Brierley et al., 2009). This has been termed the Pliocene permanent El Niño, or El Padre period (Ford et al., 2015; Wara et al., 2005).

This SST and rainfall record/projection is broadly consistent with the soil and fluvial record of the Atacama Desert. Until the mid-Miocene, when SSTs were warmer and meridional gradients are estimated to be weak, buried soils (Rech et al., 2019; Oerter et al., 2016) indicate a protracted period of salt free or carbonate bearing soils and a period when supergene enrichment was widely prevalent (Fig. 13). Additionally, deposition of fluvial deposits occurred in the northern Atacama Desert (Jordan et al., 2014; Evenstar et al., 2017; see also Fig. 13). After ca. 12-10 Ma, SSTs began a significant decline, which is interpreted to weaken Hadley circulation and increase aridity (Herbert et al., 2016). Buried paleosols in the region then consistently show protracted episodes of hyperaridity through large and deep accumulations of sulfate (Rech et al., 2019; Blanco and Tomlinson, 2013). In the late Miocene-early Pliocene, SSTs stabilized and meridional gradients declined, coincident with what has been proposed to be a permanent El Niño. During this time, two fluvial erosion and deposition episodes occurred in the northern Atacama (Jordan et al., 2014; and Unit 6 of Evenstar et al., 2017). Additionally, this time interval represents the initial climate conditions to which the alluvial deposits examined here were exposed and thus are consistent with the early-stage chemical weathering that the soils experienced. It is also coincident with the last appearance of supergene enrichment in the region (Fig. 13). The Plio-Pleistocene boundary was a time of fluvial deposition in the northern Atacama (Jordan et al., 2014) and a significant (and final) erosional/depositional cycle in the southern Atacama desert (Amundson et al., 2012a). Following this fluvial event, SSTs decline and display a shift into the present ENSO cycle characterizing the southern Pacific today (Wara et al., 2005; Revalo et al., 2006). Soil formed into these ca. 2 Ma fluvial deposits in the southern Atacama desert reveal no evidence of any chemical weathering, and record only vast quantities of salt and dust accumulation over a protracted period (Ewing et al., 2006).

The emerging picture of Atacama Desert rainfall, and the processes that the rainfall drives, appears to be converging in a manner that suggests significant changes over vast periods of time and a pattern in concert with global- and regional-scale changes in sea temperatures and atmospheric circulation (Herbert et al., 2016). These teleconnections also have important, yet not well understood, possible implications for rainfall in the warming climate of today (Burls and Fedorov, 2017).

# CONCLUSIONS

Earth's land surface is a mosaic of landforms of differing ages, and the geochemical alteration of these landforms contains an integrated record of the processes it has experienced. Developing methods to decipher this record, in situations where long-term preservation of landforms of diverse ages makes it feasible, was an objective of this research. Additionally, the field location is one that reflects climate changes that have global relationships and significance. While the Atacama Desert has a sedimentary record impoverished in fossils or botanical remains, it has considerable geological and pedological wealth due to the episodic and extended periods of great aridity that have impacted it and that have in turn preserved significant portions of it. Our research approach and results, combined with work by multiple teams, appears to be distilling into a consistent and complementary framework, one that reveals multiple periods of hyperaridity and multiple periods of more humid conditions that vary in concert with global oceanic and global climatic changes.

This present view is far from complete. For example, do buried soils have geochemical evidence of both weathering and salt accumulation,

like the relict surface soils do? Can the buried soil record be expanded, and chronologically refined, to provide better comparisons to marine records? The use of cosmogenic isotopes in buried soils might help to constrain exposure histories prior to burial and add information on the duration of hyperarid soil forming intervals. There are still uncertainties as to how the physical accretion of salts and dust over vast amounts of time, and the associated impacts of water, affect particle mixing and movement that in turn have impacts on the distribution of cosmogenic radionuclides in relict soils. These, and other, avenues of enquiry will challenge the next generation, and beyond, of earth scientists. Most importantly, relict soils have a much broader potential to understand planetary history, whether it be other locations on Earth, or other terrestrial planets such as Mars (Amundson, 2018).

#### ACKNOWLEDGMENTS

Funding for this research was provided by National Science Foundation grants 0447411 and 0819972, and by the University of California Agricultural Experiment Station, to R. Amundson. The work, over the past decades, has been greatly helped by the advice and collaboration of Guillermo Chong. We thank Greg Balco for contributions to the cosmogenic nuclide analyses. Teresa Jordan provided insight into the climate history of the desert.

#### REFERENCES CITED

- Alpers, C.N., and Brimhall, G.H., 1988, Middle Miocene climatic change in the Atacama Desert, northern Chile: Evidence from supergene mineralization at La Escondida: Geological Society of America Bulletin, v. 100, p. 1640-1656, https://doi.org/10.1130 /0016-7606(1988)100<1640:MMCCIT>2.3.CO;2.
- Amundson, R., 2018, Meteoric water alteration of soil and landscapes at Meridiani Planum, Mars: Earth and Planetary Science Letters, v. 488, p. 155–167, https://doi.org/10.1016/j.epsl.2018.02.012.
- Amundson, R., Dietrich, W., Bellugi, D., Ewing, S., Nishiizumi, K., Owen, J., Finkel, R., Heimsath, A., Stewart, B., and Caffee, M., 2012a, Geomorphic evidence for the late Pliocene onset of hyperaridity in the Atacama Desert: Geological Society of America Bulletin, v. 124, p. 1048–1070, https://doi.org/10.1130/B30445.1.
- Amundson, R., Barnes, J.D., Ewing, S., Heimsath, A., and Chong, G., 2012b, The stable isotope composition of halite and sulfate of hyperarid soils and its relation to aqueous transport: Geochimica et Cosmochimica Acta, v. 99, p. 271–286, https://doi.org/10.1016/j.gca.2012.04.044.
- Arancibia, G., Matthews, S.J., and Pérez de Arce, C., 2006, K–Ar and <sup>40</sup>Ar/<sup>39</sup>Ar geochronology of supergene processes in the Atacama Desert, Northern Chile: Tectonic and climatic relations: Journal of the Geological Society, v. 163, p. 107–118, https://doi.org/10.1144/0016-764904-161.
- Balco, G., and Shuster, D.L., 2009, Production rate of cosmogenic Ne-21 in quartz estimated from Be-10, Al-26, and Ne-21 concentrations in slowly eroding Antarctic bedrock surfaces: Earth and Planetary Science Letters, v. 281, p. 48–58, https://doi.org/10.1016/j.epsl.2009.02 006
- Bernhard, N., et al., 2018, Pedogenic and microbial interactions to regional climate and local topography: New insights from a climate gradient (arid to humid) along the Coastal Cordillera of Chile: Catena, v. 170, p. 335–355, https://doi.org/10.1016/j.catena.2018.06.018.
- Blanco, P.N., and Tomlinson, A.J., 2013, Carta Guatacondo, Regíon de Tarapacá, in Carta Geológica de Chile: San-

- tiago de Chile, Servicio Nacional Geología y Minería, Serie Geología Basica, no. 156, scale 1:100,000, 1 sheet, 116 p. text.
- Bouzari, F., and Clark, A., 2002, Anatomy, evolution, and metallogenic signature of the supergene orebody of the Cerro Colorado porphyry copper deposit, I Región, Northern Chile: Economic Geology, v. 97, p. 1701– 1740, https://doi.org/10.2113/gsecongeo.97.8.1701.
- Brierley, C.M., Fedorov, A.V., Liu, Z., Herbert, T.D., Lawrence, K.T., and LaRiviere, J.P., 2009, Greatly expanded tropical warm pool and weakened Hadley circulation in the early Pliocene: Science, v. 323, p. 1714–1718, https://doi.org/10.1126/science.1167625.
- Brimhall, G.H., and Dietrich, W.E., 1987, Constitutive mass balance relations between chemical composition, volume, density, porosity, and strain in metasomatic hydrochemical systems: Results on weathering and pedogenesis: Geochimica et Cosmochimica Acta, v. 51, p. 567–587, https://doi.org/10.1016/0016 -7037(87)90070-6.
- Burls, N.J., and Fedorov, A.V., 2017, Wetter subtropics in a warmer world: Contrasting past and future hydrological cycles: Proceedings of the National Academy of Sciences of the United States of America, v. 114, p. 12,888–12,893, https://doi.org/10.1073/pnas .1703421114.
- Cereceda, P., Larrain, H., Osses, P., Farías, M., and Egaña, I., 2008, The climate of the coast and fog zone in the Tarapacá region, Atacama Desert, Chile: Atmospheric Research, v. 87, p. 301–311, https://doi.org/10.1016/j .atmosres.2007.11.011.
- Cetiner, Z.S., Wood, S.A., and Gammons, C.H., 2005, The aqueous geochemistry of the rare earth elements. Part XIV. The solubility of rare earth element phosphates from 23 to 150 °C: Chemical Geology, v. 217, p. 147– 169, https://doi.org/10.1016/j.chemgeo.2005.01.001.
- de Porras, M.E., Maldonado, A., De Pol-Holz, R., Latorre, C., and Beancourt, J.L., 2017, Late Quaternary environmental dynamics in the Atacama Desert reconstructed from rodent midden pollen records: Journal of Quaternary Science, v. 32, p. 665–684, https://doi.org/10.1002 /jqs.2980.
- dos Santos, J.C.B., Le Pera, E., de Oliveira, C.S., de Souza Júnior, V.S., de Araújo Pedron, F., Corrêa, M.M., and de Azevedo, A.C., 2019, Impact of weathering on REE distribution in soil-saprolite profiles developed on orthogneisses in Borborema Province, NE Brazil: Geoderma, v. 347, p. 103–117, https://doi.org/10.1016/ /j.geoderma.2019.03.040.
- Ebeling, A., Oerter, E., Valley, J.W., and Amundson, R., 2016, Relict soil evidence for profound quaternary aridification of the Atacama Desert, Chile: Geoderma, v. 267, p. 196–206, https://doi.org/10.1016/j.geoderma .2015.12.010.
- Evenstar, L.A., Mather, A.E., Hartley, A.J., Stuart, F.M., Sparks, R.S.J., and Cooper, F.J., 2017, Geomorphology on geologic timescales: Evolution of the late Cenozoic Pacific paleosurface in Northern Chile and Southern Peru: Earth-Science Reviews, v. 171, p. 1–27, https://doi.org/10.1016/j.earscirev.2017.04.004.
- Ewing, S.A., Sutter, B., Owen, J., Nishiizumi, K., Sharp, W., Cliff, S.S., Perry, K., Dietrich, W.E., McKay, C.P., and Amundson, R., 2006, A threshold in soil formation at Earth's arid-hyperarid transition: Geochimica et Cosmochimica Acta, v. 70, p. 5293–5322, https://doi.org/ /10.1016/j.gca.2006.08.020.
- Ewing, S.A., Michalski, M., Thiemens, M., Quinn, R.C., Macalady, J.L., Kohl, S., Wankel, S.D., Kendall, C., McKay, C.P., and Amundson, R., 2007, Rainfall limit of the N cycle on Earth: Global Biogeochemical Cycles, v. 21, https://doi.org/10.1029/2006GB002838.
- Ewing, S.A., Yang, W., DePaolo, D.J., Michalski, G., Kendall, C., Stewart, B.W., Thiemens, M., and Amundson, R., 2008a, Non-biological fractionation of stable Ca isotopes in soils of the Atacama Desert, Chile: Geochimica et Cosmochimica Acta, v. 72, p. 1096–1110, https://doi.org/10.1016/j.gca.2007.10.029.
- Ewing, S.A., Macalady, J.L., Warren-Rhodes, K., McKay, C.P., and Amundson, R., 2008b, Change in the soil C cycle at the arid-hyperarid transition in the Atacama Desert: Journal of Geophysical Research: Biogeosciences, v. 113, https://doi.org/10.1029/2007JG000495.

- Fernández-Mort, A., Riquelme, R., Alonso-Zarza, A.M., Campos, E., Bissig, T., Mpodozis, C., Carretier, S., Herrera, C., Tapia, M., Pizarro, H., and Muñoz, S., 2018, A genetic model based on evapoconcentration for sediment-hosted exotic-Cu mineralization in arid environments: The case of the El Tesoro Central copper deposit, Atacama Desert, Chile: Mineralium Deposita, v. 53, p. 775–795, https://doi.org/10.1007/s00126-017-0780-2.
- Ford, H.L., Ravelo, A.C., Dekens, P.S., LaRiviere, J.P., and Wara, M.W., 2015, The evolution of the equatorial thermocline and the early Pliocene El Padres mean state: Geophysical Research Letters, v. 42, p. 4878–4887, https://doi.org/10.1002/2015GL064215.
- Gromet, L.P., and Silver, L.T., 1983, Rare earth element distributions among minerals in a granodiorite and the petrogenetic implications: Geochimica et Cosmochimica Acta, v. 47, p. 925–939, https://doi.org/10.1016 //0016-7037(83)90158-8.
- Hartley, A.J., and May, G., 1998, Miocene gypcretes from the Calama Basin, northern Chile: Sedimentology, v. 45, p. 351–364, https://doi.org/10.1046/j.1365-3091 .1998.0166e.x.
- Herbert, T.D., Lawrence, K.T., Tzanova, A., Peterson, L.C., Caballero-Gill, R., and Kelly, C.S., 2016, Late Miocene cooling and the rise of modern ecosystems: Nature Geoscience, v. 9, p. 843–847, https://doi.org/10.1038/ngeo2813.
- Houston, J., 2006, Variability of precipitation in the Atacama Desert: Its causes and hydrological Impacts: International Journal of Climatology, v. 26, p. 2181–2198, https://doi.org/10.1002/joc.1359.
- Jordan, T.E., Kirk-Lawlor, N.E., Blanco, P.N., Rech, J.A., and Cosentino, N.J., 2014, Landscape modification in response to repeated onset of paleoclimate states since 14 Ma, Atacama Desert, Chile: Geological Society of America Bulletin, v. 126, p. 1016–1046, https://doi.org /10.1130/B30978.1.
- Jungers, M.C., Heimsath, A.M., Amundson, R., Balco, G., Shuster, D., and Chong, G., 2013, Active erosion-deposition cycles in the hyperarid Atacama Desert of northern Chile: Earth and Planetary Science Letters, v. 371–372, p. 125–133, https://doi.org/10.1016/j.epsl.2013.04.005.
- Kohl, C.P., and Nishiizumi, K., 1992, Chemical isolation of quartz for measurement of in situ produced cosmogenic nuclides: Geochimica et Cosmochimica Acta, v. 56, p. 3583–3587, https://doi.org/10.1016/0016 -7037(92)90401-4.
- Lal, D., 1991, Cosmic ray labeling of erosion surfaces: In situ nuclide production rates and erosion models: Earth and Planetary Science Letters, v. 104, p. 424–439, https://doi.org/10.1016/0012-821X(91)90220-C.
- Lear, C.H., Elderfield, H., and Wilson, P.A., 2000, Cenozoic deep-sea temperatures and global ice volumes from Mg/Ca in benthic foraminiferal calcite: Science, v. 287, p. 269–272, https://doi.org/10.1126/science.287 .5451.269.
- Marinovic, N., Smoje, I., Maksaev, V., Herve, M., Mpodozis, C., 1992, Hoja Aguas Blancas, Región de Antofagasta: Servicio Nacional de Geología y Minería, Carta Geológica de Chile, no. 70, scale 1:250,000, 150 p.
- Marsh, T.M., Einaudi, M.T., and McWilliams, M., 1997, <sup>40</sup>Ar/<sup>39</sup>Ar geochronology of Cu-au and Au-Ag mineralization in the Potrerillos District Chile: Economic Geology, v. 92, p. 784–806, https://doi.org/10.2113/ /gsecongeo.92.7-8.784.
- McFadden, L.D., Wells, S.G., and Jercinovich, M.J., 1987, Influences of eolian and pedogenic processes on the origin and evolution of desert pavements: Geology, v. 15, p. 504–508, https://doi.org/10.1130 /0091-7613(1987)15<504:IOEAPP>2.0.CO;2.
- Michalski, G., Bohlke, J.K., and Thiemens, M., 2004, Long term atmospheric deposition as the source of nitrate and other salts in the Atacama Desert, Chile: New evidence from mass-independent oxygen isotopic compositions: Geochimica et Cosmochimica Acta, v. 68, p. 4023– 4038, https://doi.org/10.1016/j.gca.2004.04.009.
- Minařík, L., Žigová, A., Bendl, J., Skřivan, P., and Šťastnýd, M., 1998, The behaviour of rare-earth elements and Y during the rock weathering and soil formation in the Říčany granite massif, Central Bohemia: The Science

- of the Total Environment, v. 215, p. 101–111, https://doi.org/10.1016/S0048-9697(98)00113-2.
- Mortimer, C., 1973, The Cenozoic history of the southern Atacama Desert, Chile: Journal of the Geological Society, v. 129, p. 505–526, https://doi.org/10.1144/gsjgs .129.5.0505.
- Moscoso, R., Nasi, C., and Salinas, P., 1982, Geología de la Hoja Vallenar y parte Norte de La Serena, Regiones de Atacama y Coquimbo: Santiago de Chile, Servicio Nacional Geología y Minería, Carta Geológica de Chile no. 55, scale 1:250,000.
- Mote, T.I., Becker, T.A., Renne, P., and Brimhall, G.H., 2001, Chronology of exotic mineralization at El Salvador, Chile, by <sup>40</sup>Ar/<sup>59</sup>Ar dating of copper wad and supergene alunite: Economic Geology, v. 96, p. 351–366, https://doi.org/10.2113/gsecongeo.96.2.351.
- Muñoz-Farías, S., Ritter, B., Dunai, T.J., Morales-Leal, J., Campos, E., Spikings, R., and Riquelme, R., 2023, Geomorphological significance of the Atacama Pediplain as a marker for the climatic and tectonic evolution of the Andean forearc, between 26° to 28°S: Geomorphology, v. 420, https://doi.org/10.1016/j.geomorph.2022 .108504.
- Navarro-González, R., Rainey, F.A., Molina, P., Bagaley, D.R., Hollen, B.J., de la Rosa, J., Small, A.M., Quinn, R.C., Grunthaner, F.J., Caceres, L., Gomez-Silva, B., and McKay, C.P., 2003, Mars-like soils in the Atacama Desert, Chile, and the dry limit of microbial life: Science, v. 302, p. 1018–1021, https://doi.org/10.1126 /science.1089143.
- Nesbitt, H.W., 1979, Mobility and fractionation of rare earth elements during weathering of a granodiorite: Nature, v. 279, p. 206–210, https://doi.org/10.1038/279206a0.
- Nishiizumi, K, 2004, Preparation of <sup>26</sup>Al AMS standards: Nuclear Instruments and Methods in Physics Research Section B: Beam Interactions with Materials and Atoms, v. 223–224, p. 388–392, https://doi.org/10.1016 /j.nimb.2004.04.075.
- Nishiizumi, K., Imamura, M., Caffee, M.W., Southon, J.R., Finkel, R.C., and McAninch, J., 2007, Absolute calibration of <sup>10</sup>Be AMS standards: Nuclear Instruments and Methods in Physics Research, v. 258, p. 403–413, https://doi.org/10.1016/j.nimb.2007.01.297.
- Oerter, E., Amundson, R., Heimsath, A., Jungers, M., Chong, G., and Renne, P., 2016, Early to middle Miocene climate in the Atacama Desert of northern Chile: Palaeogeography, Palaeoclimatology, Palaeoecology, v. 441, p. 890–900, https://doi.org/10.1016/j.palaeo.2015.10.038.
- Oeser, R.A., and von Blanckenburg, F., 2020, Strontium isotopes trace biological activity in the Critical Zone along a climate and vegetation gradient: Chemical Geology, v. 558, https://doi.org/10.1016/j.chemgeo.2020 .119861.
- Owen, J.J., Amundson, R., Dietrich, W.E., Nishiizumi, K., Sutter, B., and Chong, G., 2011, The sensitivity of hillslope bedrock erosion to precipitation: Earth Surface Processes and Landforms, v. 36, p. 117–135, https://doi .org/10.1002/esp.2083.
- Pfeiffer, M., Morgan, A., Heimsath, A., Jordan, T., Howard, A., and Amundson, R., 2021, Century scale rainfall in the absolute Atacama Desert: Landscape response and implications for past and future rainfall: Quaternary Science Reviews, v. 254, https://doi.org/10.1016 /j.quascirev.2021.106797.
- Placzek, C., Granger, D.E., Matmon, A., Quade, J., and Ryb, U., 2014, Geomorphic process rates in the central Atacama Desert, Chile: Insights from cosmogenic nuclides and implications for the onset of hyperaridity: American Journal of Science, v. 314, p. 1462–1512, https://doi .org/10.2475/10.2014.03.
- Quade, J., Rech, J.A., Latorre, C., Beancourt, J.L., Gleeson, E., and Kalin, M.T.K., 2007, Soils at the hyperarid margin: The isotopic composition of soil carbonate from the Atacama Desert, northern Chile: Geochimica et Cosmochimica Acta, v. 71, p. 3772–3795, https://doi .org/10.1016/j.gca.2007.02.016.
- Railsback, L.B., 2003, An earth scientist's periodic table of the elements and their ions: Geology, v. 31, p. 737–740, https://doi.org/10.1130/G19542.1.

- Rech, J.A., Quade, J., and Hart, W.S., 2003, Isotopic evidence for the source of Ca and S in soil gypsum, anhydrite, and calcite in the Atacama Desert, Chile: Geochimica et Cosmochimica Acta, v. 67, p. 575–586, https://doi.org /10.1016/S0016-7037(02)01175-4.
- Rech, J.A., Currie, B.S., Michalski, G., and Cowan, A.M., 2006, Neogene climate change and uplift in the Atacama Desert, Chile: Geology, v. 34, p. 761–764, https://doi.org/10.1130/G22444.1.
- Rech, J.A., Currie, B., Jordan, T.E., Riquelme, R., Lehmann, S.B., Kirk-Lawlor, N.E., Li, S., and Gooley, J.T., 2019, Massive middle Miocene gypsic paleosols in the Atacama Desert and the formation of the Central Andean rain-shadow: Earth and Planetary Science Letters, v. 506, p. 184–194, https://doi.org/10.1016/j.epsl.2018.10.040.
- Revalo, A.C., Dekens, P.S., and McCarthy, M., 2006, Evidence for El Niño-like conditions during the Pliocene: GSA Today, v. 16, no. 3, p. 4–11, https://doi.org/10.1130/1052-5173(2006)016<4:EFENLC>2.0.CO:2.
- Sharma, P., Bourgeois, M., Elmore, D., Granger, D., Lipschutz, M.E., Ma, X., Miller, T., Mueller, K., Rickey, F., Simms, P., and Vogt, S., 2000, PRIME lab AMS performance, upgrades and research applications: Nuclear Instruments & Methods in Physics Research Section B: Beam Interactions with Materials and Atoms, v. 172, p. 112–123, https://doi.org/10.1016/S0168-583X(00)00132-4.
- Sillitoe, R.H., and McKee, E.H., 1996, Age of supergene oxidation and enrichment in the Chilean porphyry copper province: Economic Geology, v. 91, p. 164–179, https://doi.org/10.2113/gsecongeo.91.1.164.
- Vasconcelos, P.M., Reich, M., and Shuster, D.L., 2015, The paleoclimatic signatures of supergene metal deposits: Elements, v. 11, p. 317–322, https://doi.org/10.2113/gselements.11.5.317.
- Vermeesch, P., 2007, CosmoCalc: An Excel add-in for cosmogenic nuclide calculations: Geochemistry, Geophysics, Geosystems, v. 8, https://doi.org/10.1029/2006GC001530.
- Vermeesch, P., Balco, G., Blard, P.-H., Dunai, T.J., Kober, F., Niedermann, S., Shuster, D.L., Strasky, S., Stuart, F.M., Wieler, R., and Zimmermann, L., 2015, Interlaboratory comparison of cosmogenic <sup>21</sup>Ne in quartz: Quaternary Geochronology, v. 26, p. 20–28, https://doi.org/10.1016/j.quageo.2012.11.009.
- Wang, F., Michakski, G., Seo, J.H., Granger, D.E., Lifton, N., and Caffee, M., 2015, Beryllium-10 concentrations in the hyper-arid soils of the Atacama Desert, Chile: Implications for arid soil formation rates and El Niño driven changes in Pliocene precipitation: Geochimica et Cosmochimica Acta, v. 160, p. 227–242, https://doi.org /10.1016/j.gca.2015.03.008.
- Wara, M.W., Ravelo, A.C., and DeLaney, M.L., 2005, Permanent El Niño-like conditions during the Pliocene warm period: Science, v. 309, p. 758–761, https://doi.org/10.1126/science.1112596.
- Welsh, H., Gueorguieva, G.A., Kounaves, S., and Amundson, R., 2020, Stable nitrogen and oxygen isotope fractionation during precipitation of nitrate salt from saturated solutions: Rapid Communications in Mass Spectrometry, v. 34, https://doi.org/10.1002/rcm.8905.
- Yi-Balan, S.A., Amundson, Ř., and Buss, H.L., 2014, Decoupling of sulfur and nitrogen cycling due to biotic processes in a tropical rainforest: Geochimica et Cosmochimica Acta, v. 142, p. 411–428, https://doi.org/10 .1016/j.gca.2014.05.049.
- Zhang, Y.G., Pagani, M., and Liu, Z., 2014, A 12-million-year temperature history of the tropical Pacific Ocean: Science, v. 344, no. 6179, p. 84–87, https://doi.org/10.1126/science.1246172.

SCIENCE EDITOR: MIHAI DUCEA ASSOCIATE EDITOR: EMMANUEL GABET

Manuscript Received 25 September 2023 Revised Manuscript Received 10 June 2024 Manuscript Accepted 28 June 2024